

CHAPTER III

INSTRUMENTAL DETAILS

&

EXPERIMENTAL TECHNIQUE

III.1 Techniques of Measurement :

The reaction cross sections can be measured using any of the following two techniques:

- (i) In-beam or on-line technique.
- (ii) Off-beam or off-line technique.

III.1.1 In-beam Technique :

This is the technique in which the irradiation of the target and the detection of radiations emitted from the product nuclei, is done simultaneously. To study the cross section of a particular reaction, we analyse the prompt gamma rays spectra associated with the reaction. The decay scheme of the residual nuclei should be well known. Due to complex gamma ray spectra, some times gamma-gamma coincidences are also necessary for the proper identification of the gamma rays. The gamma ray detector should be well shielded so that back ground neutrons emitted in the reaction may not damage the detector.

III.1.2 Off-beam Technique :

In this technique the target is irradiated first, after that the analysis of product nuclei is done. That is why this technique is also name as activation technique. The beta or gamma activities associated with the product nucleus can be studied by using the appropriate detectors. It is very much advantageous technique because in this technique the reaction cross section at several incident energies can be studied with a single irradiation by arranging the target foils in the form of a stack. On the other hand this technique is limited to those isotopes only, which are stable but their product nuclides are unstable and have convenient half lives because

the detection of radiation coming from the product nuclei and the irradiation of the target nuclei are done separately so there is some lapse of time between those two processes. If the half life of the product nucleus is very short, then the activity due to this product nucleus will decay out. Moreover, the decay scheme of the product nuclei should be properly established. We have many advantages inherent in this technique due to high sensitivity with which this induced activity can be detected the individual characteristic modes of decay of each radio-isotope. Some of the particular advantages are; extremely high sensitivity, selectivity and possibility of non-destructive analysis. Presently, the off-line technique has been used for the cross section measurements.

III.2 Outline of Radiation Detection :

Radiation detectors play a very important role in any experimental nuclear research programme. They provide information on the type, energy and multiplicity of the radiations emitted in a nuclear reaction. The basic requirement for any detector is a high detection efficiency and a good energy resolution. The detector technology, in its turn, has been rapidly evolving, making use of the latest developments in material processing, detector design, fabrication technology etc, thus making the best detectors of today, no longer the detectors of choice tomorrow.

In the activation technique, employed in the present work, two methods can be used for the study of the activated sample:

- 1) Beta counting method and
- 2) Gamma counting method

A survey of the literature data indicates that the large uncertainties of a number of results possibly arise from the detecting technique employed. Earlier, the beta activity and gamma activity measurements were carried out using G.M. Counter and NaI(Tl) scintillation spectrometers respectively. The beta measurements were limited to the use of thin samples, since self-absorption and self-scattering effects are considerable for beta rays. Some of these measurements resulted in too high cross section values, since interfering contributions from other reactions could not be effectively separated.

The difficulties with the beta counters could be overcome by using NaI(Tl) detector which are used to measure the induced gamma activities in the irradiated sample. Though the efficiency is good, NaI(Tl) systems have inadequate resolution in as much as closely lying gamma energies could not be differentiated. In the present work, with alpha particles upto 50 MeV, a large number of reactions are energetically possible in each target element and the gamma ray spectra are expected to be very complex. To resolve the different gamma ray peaks of these reactions, even the NaI(Tl) crystals having best resolution (8-10% for 662 keV photons of Cs¹³⁷) are hardly useful. Besides, the analysis of gamma spectra recorded on a NaI(Tl) spectrometer is associated with considerable errors due to the large Compton background arising from high energy gamma rays and due to the presence of escape and back-scattering peaks.

Some of the above factors may have been responsible for the observed discrepancies in the cross section data reported by different authors. Keeping this in view, the present measurements are carried out employing gamma counting technique with a high resolution large volume coaxial germanium detector, anticipating more reliable and more precise results compared to the earlier work. As a matter of fact, it is worth reinvestigating, with a germanium detector, each reaction

cross section that was earlier measured with either a G.M.Counter or a NaI(Tl) scintillation spectrometer or Ge(Li) detector.

Besides the excellent resolution, the germanium detectors have the following advantages:

- 1) Linear response over a wide range of gamma energies
- 2) Insensitivity of pulse to counting rate
- 3) Fast pulse rise time
- 4) Less pronounced back scattering and escape peaks, and finally
- 5) High full-energy peak to Compton background ratio

In the following brief description of the experimental set up, consisting of a Ge-spectrometer with the associated electronic modules and its calibration; data collection and data reduction is presented.

III.2.1 Ge (Li) Detector for High Resolution Gamm-ray Spectroscopy :

The development of semiconductor radiation detectors revolutionised various branches of physics. A semiconductor detector is nothing but a highly doped p-n junction with an intrinsic region formed at the junction. It is this intrinsic region which acts as the sensitive volume of the detector. The fabrication process of a Ge(Li) detector is a well known procedure and found extensively in literature /1/. Lithium is drifted in a p-type germanium crystal at 425°C for about five minutes to get sufficient concentration of Lithium in the n⁺ layer for drifting. Once the drifting process is completed, which takes several days, the region between n⁺ layer and the uncompensated p- region simply called the “intrinsic region” or “depletion region” is the active region or sensitive volume of the detector. Since the stopping power of

a solid is much higher than that of a gas, even a few cc of the sensitive volume of a solid state radiation detector is sufficiently efficient. The earlier type of solid state detectors were of surface barrier type with intrinsic region of only a few hundred microns thick. They were suitable for heavy charged particles like protons, alpha particles etc. For the detection of electrons and gamma rays thicker intrinsic regions are developed by Tevendale and Ewan /1/ made it possible to realise large sensitive volumes. Later on coaxial type of detectors were developed to enable the production of large sensitive volumes. The truly coaxial geometry provides uniform charge collection fields and results in a fast uniform pulse rise time that is well suited to fast-timing experiments. The Ge detectors are cooled to liquid nitrogen temperature of 77°K to reduce thermally generated leakage current to acceptable values. This is because of the fact that the lithium ions have large mobility in germanium at room temperature and this cause redistribution of the lithium ions from the compensated region spoiling the operational characteristics of the detector. In order to maintain the Ge(Li) detectors at liquid nitrogen temperature, these are enclosed in a vacuum cryostat and a dewar filled with liquid nitrogen. Thus in the maintenance of Ge(Li) detector extreme care has to be taken to see that the dewar, in which cryostat housing the detector is dipped, is regularly filled with liquid nitrogen. The vertical portion of the cryostat holds the cryosorption molecular sieve pellets. These pellets when cooled to liquid nitrogen temperature maintain vacuum at a reasonable level. If accidentally the Ge(Li) detector comes to room temperature then due to the loss of compensation the basic structure of the detector is damaged thereby rendering the detector unworkable.

III.2.2 High Purity Germanium Detector :

With the advances in the crystal growth technology , it has been possible to grow large size germanium crystals with a very high degree of purity (i.e. the

impurity concentration in the range of 10^9 to 10^{11} atoms / cc). Thus, it has become possible to fabricate thick detectors without lithium compensation from the available high purity germanium .An important consequence is that these high purity Ge detectors do not have to be maintained permanently at liquid nitrogen temperature after fabrication. In the case of Li-doped, i.e. Ge(Li) detectors, it is necessary to keep the detectors always cooled , to avoid migration of Li by diffusion process, which would eventually lead to incomplete and inadequate compensation. With the new high purity Ge detector, they may stored (still in their vacuum-tight encapsulations) at room temperature and only need to be cooled to liquid nitrogen temperature when in use.

The raw material for HPGe detectors is p-type Czochralski grown single crystal germanium having impurity concentration of the order of 10^{10} atoms/cc. Also, while fabricating HPGe detectors, extreme care is to be taken. The n^+ contact is formed by lithium diffusion at some what lower temperature (~ 200 $^{\circ}\text{C}$) than those used in fabricating Ge(Li) detectors. The surface barrier (p^+) contact is applied to the axial hole by evaporation of an appropriate material like gold, platinum, chromium or palladium. This results in a $n^+ - p - p^+$ configuration in which the depletion region is formed by reverse biasing the n^+p junction. Since, there is a significant dead layer on the n^+ face, the p^+ face is normally used as the entrance window. The electric field strength across the windows region must be sufficient to collect the electron-hole pairs produced from photon interactions.

III.2.3 γ - ray Detection in Semiconductor Detector :

Interaction of nuclear radiation with matter results in a deposition of energy in the medium traversed by the radiation. Radiation detection relies on the sensing of this energy deposition through some suitable means. The collection of the free

charges released in the medium resulting in a current or voltage pulse and the detection of the photons emitted during the deexcitation of the excited or ionised atoms and molecules along the path of the incident radiations, are two most convenient ways to sense the energy deposition.

The detection of the charge particles is based on the direct ionisation produced along its path in the active region. The electron-hole pairs produced are swept across by the detector bias. The motion of the charges in the intrinsic region induces charge. Thus, the charge is collected at the detector output capacitance and it is proportional to the energy expended inside the active region of the detector. In the detection of photons, which do not directly produce ionisation, the detection is based on the secondary charged particles (electrons and positrons) produced in their interaction with the medium. At photon energies below a few MeV, the predominant modes of interaction are photo-electric effect, Compton scattering and pair production. If the photon interaction is a photo-electric interaction, the resulting photo - electron is stopped in the detector medium and the associated x-ray is also mostly reabsorbed in the detector medium. Consequently, the entire energy of the incident photon is deposited in the detector medium. If the interaction is a Compton scattering, the resulting electrons have a continuous energy distribution from 0 to maximum. If the detector is sufficiently thin, the scattered γ -rays usually escape the detector medium without further interaction. In this condition a part of the energy is deposited in the detector medium and the output pulse height shows a continuous distribution. This is usually referred to as "Compton background". If the incident γ -ray energy is sufficiently high (above 1.02 MeV) the pair production process becomes a competing interaction. The electrons and positrons created as a result of this interaction, deposit their kinetic energy in the detector medium. On slowing down, the positron annihilates resulting in the creation of two γ - photons of energy 511 keV each. Depending upon none, one or both these annihilation radiations

escaping the detector, one observes the full energy, one-escape or two-escape peaks in the spectrum for the same energy γ -rays incident on the detector.

The probability of interaction caused by γ - rays may be expressed in terms of an effective cross sectional area for each atom of the medium , as

$$1) \tau_1 \propto Z^5 / E^{3.5} \text{ (for photo - electric absorption cross section)}$$

$$2) \tau_2 \propto Z / E \text{ (for Compton absorption cross section)}$$

$$3) \tau_3 \propto Z^2 (E - 1.02) \text{ (for pair production cross section)}$$

Since $\tau_1 \propto Z^5 / E^{3.5}$, the Ge(Li) detector offers higher efficiency for photons than Si(Li) detector. The later is, however used for low energy photons and x-rays. But, since the band gap of Ge (0.66 eV) is very small compared to that of Si (1.02 eV), the former is not suitable for room temperature operation . However, good results are expected from both only when they are operated at liquid nitrogen temperatures because of the large carrier densities and corresponding leakage currents that arise at room temperature from the bulk of the material.

III.2.4 Germanium Detector Spectroscopy System :

A block diagram of the γ - ray spectrometry is given in figure.III.1. It consists of a pre-amplifier assembled with Ge detector, high voltage power supply, spectroscopy amplifier and a multichannel analyser with facilities for storage , display and typing the experimental data . A brief description of each unit is given below. The same electrical circuit for all A.C power to the system was used to avoid ground loops. The bias supply and amplifier were located on opposite ends of the bin , to minimise cross talk between them.

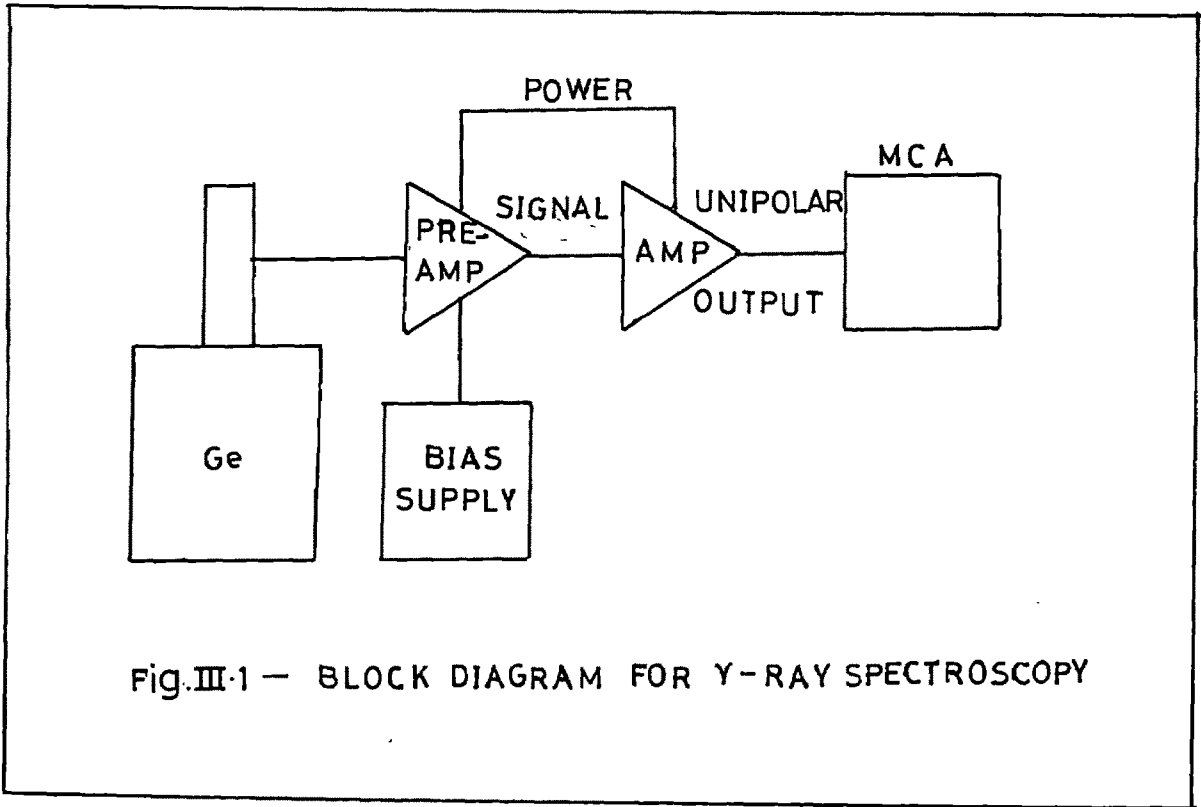


Fig.III-1 — BLOCK DIAGRAM FOR γ -RAY SPECTROSCOPY

Pre-amplifier : For GM tubes and other ionisation detectors the charge liberated by the incident radiation is sufficient to produce a large signal pulse. In case of semi conductor detectors, the charge is so small that without any intermediate amplification step , it is not possible to deal with the signal pulses. The first element in a signal processing chain is a pre- amplifier working as an interface between the detector and the pulse processing electronics. The pre- amplifier is kept as close to the detector as possible , to minimise the capacitive loading on the detector , by avoiding long interconnecting cables between the detector and pre-amplifier. Thus a maximum peak-to noise ratio can be achieved, by quickly terminating the capacitance. A field effect transistor (FET) which serves as the first stage of the amplifier is cooled to liquid nitrogen temperature for its proper function. For this reason the pre-amplifier is kept in thermal contact with the cryostat housing the detector. Noise in charge sensitive pre-amplifiers is generally controlled by three components: the input Field Emission Transistor (FET), the input capacitance (the detector capacitance, the cabling capacitance, etc.) and the resistance connected to the input.

Both the detectors [Ge(Li) and HPGe] are associated with charge sensitive pre-amplifiers. These pre-amplifiers are preferred for most spectroscopy applications. The pre-amplifier converts the ionisation charge developed in the detector during each absorbed nuclear event to a step function pulse output whose amplitude is proportional to the total charge accumulated in that event. The sensitivity (or gain) is generally expressed in millivolts per MeV of energy deposited in a given detector material . The charge Q_D released by the detector is a function of the particle energy and the detector material and is given by

$$Q_D = E e \times 10^6 / \epsilon$$

where E is the energy of incident radiation in MeV, e is the charge of electron and ϵ is the amount of energy required to produce an electron-hole pair in the detector

(approximate value of ϵ for Ge is 2.96 eV at 77 ° K). In this class of pre-amplifiers any change in the input capacitance has no appreciable effect on the output voltage.

Amplifier : The output signal obtained from a pre-amplifier is fed to a amplifier not only to further amplify the signal but also to shape the signals to optimize spectrometer performance. The basic requirement of an amplifier is to have an optimum pulse shape, in order to enhance the signal-to-noise ratio and to make the amplification independent of variations in input pulse rise times. If the product of input amplitude and gain exceeds the maximum design output amplitude, the amplifier output pulse will saturate and produce a distorted pulse with a flat top at that amplitude. Linear amplification will be realised only for those pulses that are short of this saturation level. Hence in order to achieve an exceptionally stable performance, an amplifier with a built - in pile up rejector and a automatic base line restorer is employed for the present work. Active filter net works permit the generation of very symmetrical unipolar outputs with optimum signal to noise ratios over a wide range of time constants.

Detector Bias Supply : The detectors involved in the present work require an external high voltage for their proper operation. This voltage is conventionally called “detector bias” and the units used for this purpose are often called detector bias supply.

The detector bias supply selected should have the required voltage and polarity options and current capacity. Semiconductor detectors (HPGe/Ge(Li)) which are employed in the present work draw very little current and the high voltage does not exceed 2000 volts, but a high stabilisation factor is required.

Multichannel Analyser : The multichannel pulse height analyser (MCA) is an instrument developed to deal with the examination of each pulse coming from the main amplifier and to determine into which size category it should fit. The MCA keeps a record in its memory of how many pulses of each size it has found. The MCA presents a cathode ray tube (CRT) display of the number of counts in each channel, in effect in a histogram. The number of channels available depends upon the particular MCA, but normally ranges from 1024 to 8192.

Modern MCA's are special purpose computers whose memory addresses can be programmed to correspond to increment to voltage. Each time, a detector produces an output signal, the amplitude of signal is converted to a pulse train by the computer. These pulses are counted on an address scalar in the computer memory. The sum of the pulses produced by a given input signal equals the address in which data is to be stored. The address (proportional to the signal amplitude) is selected and a count of one added to the content of the memory at that address. The next signal from the detector is digitised and address proportional to the amplitude of the detected signal is selected, a count of one is added to the memory at that address and so on. The process continues for a duration determined by the experimenter and an energy distribution spectrum is recorded. This process is called pulse height analysis.

III.2.5 Energy Calibration of the Ge Detector :

In the off line γ -ray spectroscopy, it is necessary to adjust the spectrometer to a well defined, precise and optimum performance condition. This can be achieved by properly adjusting the associated electronic modules. One important unit is spectroscopic amplifier. The resolution of the detector can be best achieved by properly adjusting the time constant of the spectroscopy amplifier. The resolution

of the detector is defined as the full width at half maximum (FWHM) divided by the peak centroid for a given photon group. In spectroscopy amplifier there is a provision for varying the time constant from 0.25 to 8 μ s. The variation constant of the FWHM is carefully studied with the variation in time constant of the spectroscopy amplifier. In this way, an optimum and best resolution was obtained with the time constant 6 μ s . Hence throughout the course of present investigation the same time constant is used.

The next task is to calibrate the multichannel analyser. Initially this is done with the help of standard γ -ray sources like ^{60}Co , ^{137}Cs , ^{133}Ba , ^{57}Co . The prominent peaks in the back ground also serve as additional points. Intermittently, to check the calibration, the use of a multigamma source like ^{152}Eu is preferred because it covers the γ -energies from 122 keV to 1408 keV. This energy region almost covers the region of interest in the present studies. When once the calibration is done, the energy of any unknown peak appearing in the γ -spectrum can be obtained with the help of calibration equation. Normally for the limited region 100-1500 keV, a linear relation is assumed between the photon energy and the centroid of the peak. Weighted least square fitting of the calibration points gives the equation

$$E(\text{keV}) = k_1(\text{Channel Number}) + k_2$$

where k_1 is the slope of line which is nothing but energy / channel and k_2 is the intercept, representing zero point energy. So, by accurately determining the constants k_1 and k_2 , any unknown peak energy can be determined in the experimental spectrum.

III.2.6 Efficiency Calibration of Ge Detector :

Efficiency of Ge detectors is an important quantity for the determination of cross section of nuclear reactions . The accuracy of determination of this quantity

will influence the accuracy of the overall measurement. Hence, there are several points to be taken into consideration while determining the efficiency of Germanium detectors. The first thing is the geometry. One has to select a suitable geometry of the source and detector, second being the use of a multigamma source. It is advantageous to use a multigamma rays source, which emits γ -rays with different energies spread over the entire range of interest. Several such sources have been proposed in literature. With regard to half life, number, distribution and relative abundance of photons, ^{152}Eu is particularly suited for the energy region 100 to 1500 keV. The details of this nuclide are given in table III.1 as taken from literature /2,3/ .

Ge(Li)/HPGe spectroscopy is widely used for the determination of the γ -ray emission rates . If the experimenter aims at high accuracy, two types of summing corrections have to be taken into account: (i) random summing and (ii) coincidence summing. Random summing becomes important at high counting rates where pile-up leads to losses from the full energy peak /3/. Coincidence summing occurs with radio nuclides emitting two or more cascading photons within the resolving time of the detector. If for example when the first photon spends its total energy in the Ge crystal, if the second photon is also detected , a sum peak which may not correspond to either of the two full energy peaks is recorded. The probability for such summing effects decreases with increasing source - to - detector distance i.e. by using small solid angles of detector. So, by properly adjusting the count rates and geometry, the losses due to dead time, pile up and cascading effects can be reduced.

The photopeak efficiency P_γ for the detection of a gamma ray of energy E_γ in a specified geometry is

$$P_\gamma = \frac{\text{No. of } \gamma\text{-rays of energy } E_\gamma \text{ detected in the photopeak}}{\text{No. of } \gamma\text{-rays of energy } E_\gamma \text{ incident on the detector}}$$

Table III.1 ^{152}Eu gamma ray energies , their abundances and uncertainties :

Energy E_γ (keV)	Abundance per decay (θ_γ)	Uncertainty in θ_γ (%)
121.8	0.3067	0.83
244.7	0.0771	0.71
344.3	0.2720	0.68
788.9	0.1271	0.53
964.0	0.1468	0.40
1112.1	0.1376	0.41
1408.1	0.2197	0.40

$$P_{\gamma} = A_{\gamma} / S \cdot \theta_{\gamma} \, d\Omega$$

where A_{γ} is the observed photopeak area per second of the γ -ray, θ_{γ} is the absolute γ -ray intensity per decay of residual nucleus, S is the source strength given in terms of disintegration per second and $d\Omega$ is the solid angle subtended by the detector at the source.

Efficiency calibration curves are approximate straight lines when plotted on a double logarithmic plot. Excepting at very low energies (< 200 keV), the calibration points lie on a straight line in the region 200 keV to 1500 keV. Mathematically /1/,

$$P_{\gamma} = a E_{\gamma}^{-b}$$

which gives a straight line function, $\log P_{\gamma} = \log a - b \log E_{\gamma}$, where P_{γ} is the photopeak efficiency for the energy E_{γ} ; a and b are the intercept and slope on a double logarithmic plot respectively. A straight line fitting is made to the calibration points by method of weighted least squares fit /4/ as shown in figures III.2 and III.3. The best fitted line passes through the actual experimental points except at low energies (< 200 keV). Because in this low energy region the efficiency curve is not a straight line but in reality has curvature due to self absorption effects, the least squares fitted line is smoothly jointed to the low energy experimental point at 120 keV. The values of these constants a and b for each source to detector distances are given in tables III.2 and III.3.

III.3 Outline of the Experimental Procedure :

In the present investigations, the stacked foil activation technique and gamma counting method have been employed to determine the cross sections of α -particle induced reactions. Activation technique is applicable to the study of reactions in which the residual nucleus is radioactive, with a convenient half life, so

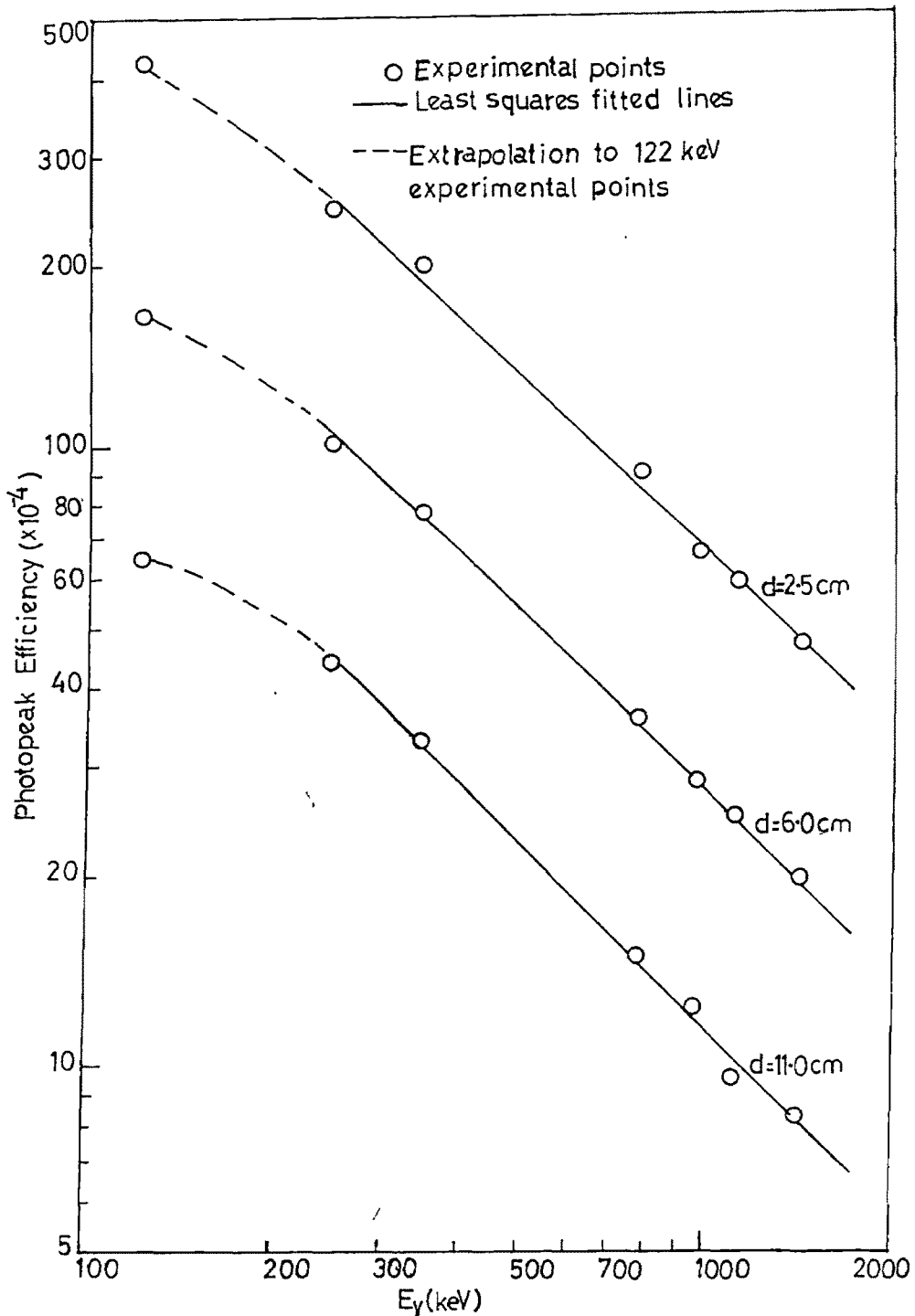


FIG.III-2 PHOTOPEAK EFFICIENCY CURVES FOR Ge(Li) DETECTOR FOR DIFFERENT SOURCE DETECTOR DISTANCES, WITH STANDARD ¹⁵²Eu SOURCE.

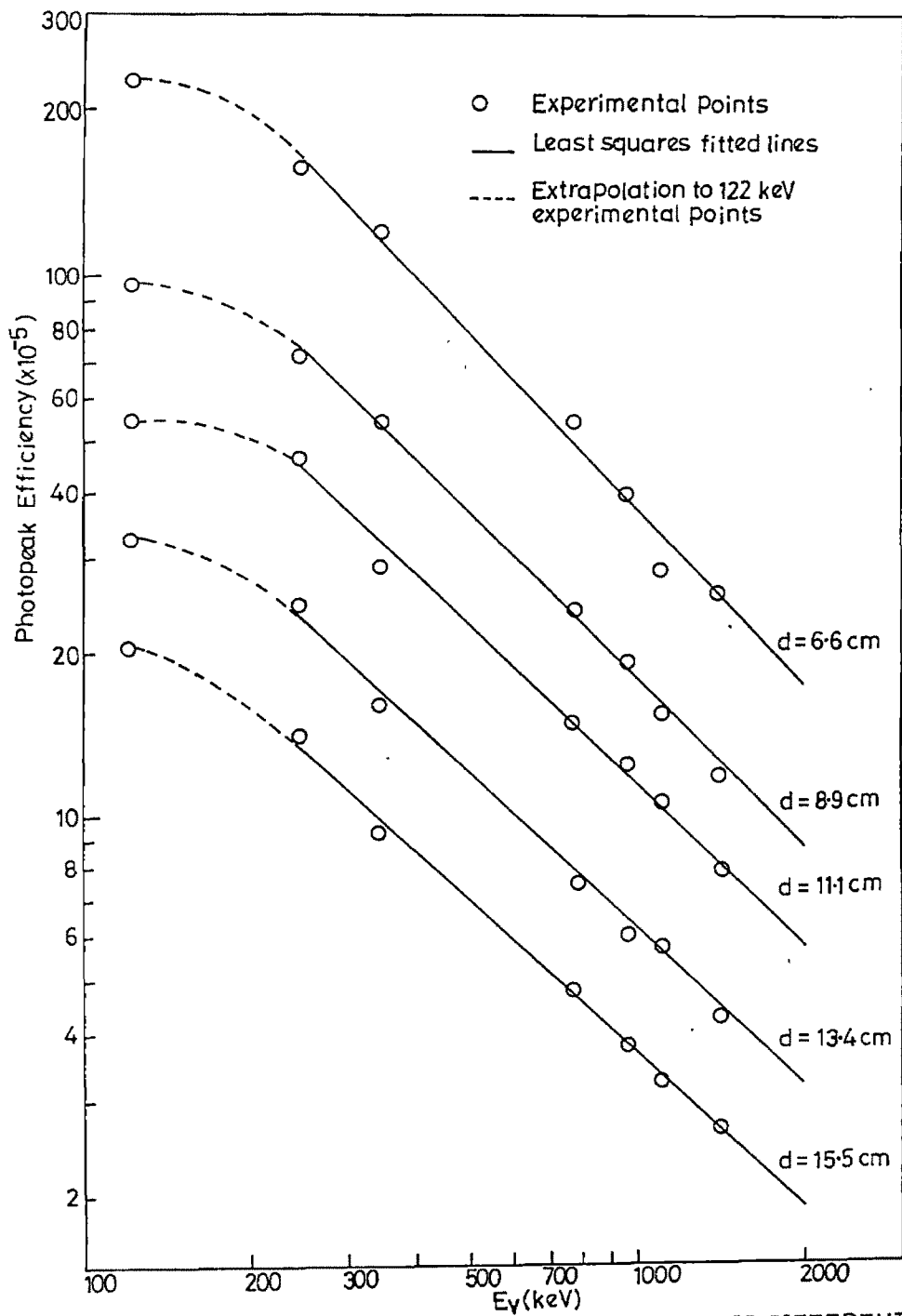


Fig.III.3 PHOTOPEAK EFFICIENCY CURVES FOR HPGe DETECTOR FOR DIFFERENT SOURCE DETECTOR DISTANCES, WITH STANDARD ^{152}Eu SOURCE.

Table III.2 Values of constant a and b for Ge(Li) detector, obtained in the weighted least squares fitting /4/ of the efficiency curve , $10^4 P_\gamma = a E_\gamma^{-b}$ on a double logarithmic calibration plot

Distance (d) cm	a	b
02.5	10.8546	-0.9648
06.0	09.8357	-0.9434
11.0	09.1399	-0.9700

Table III.3 Values of constant a and b for HPGe detector, obtained in the weighted least squares fitting /4/ of the efficiency curve , $10^5 P_\gamma = a E_\gamma^{-b}$ on a double logarithmic calibration plot

Distance (d) cm	a	b
06.6	11.0384	-1.0757
08.9	10.0039	-1.0329
11.1	09.0871	-0.9637
13.4	08.4979	-0.9722
15.5	07.7148	-0.9291

as to make the activation as well as measurement of activity feasible. However, quite many reactions are amenable, with a wide range of half lives from a few minutes to several months.

Stacked foil activation technique has the unique advantage of allowing the measurement of reaction cross section over a wide range of energy in a single irradiation. The technique consists of preparing a stack of experimental foils together with suitable aluminium degraders, to reduce the beam energy to the desired levels. As the beam passes through the successive foils of the stack, the alpha beam loses its energy but not the intensity. Hence, each experimental foil sees effectively a beam of different energy falling on it. Using the standard range energy data /5/ the precise energy of the α -particle incident on each experimental foil can be determined. The total thickness of the stack is chosen to be definitely less than the range of the primary α -particle beam in the material of the stack so that all the target foils see the same incident α -particle flux. Also care is taken to ensure that the total thickness of the stack is not too large, as there will be errors in the estimated particle energies due to straggling and also there may be some loss of beam intensity due to nuclear interaction in which the α -particles are either absorbed or removed from the beam.

Keeping these things in minds , the stacks of self supporting metallic foils of gold (Au), indium(In) and iron(Fe) of purity greater than 99.99% and of thickness 24.0 mg/cm^2 , 43.86 mg/cm^2 , 19.65 mg/cm^2 respectively were used. However, in the case of antimony(Sb), target foils were prepared by vacuum evaporation technique of thickness 1.6 mg/cm^2 at the target division of Variable Energy Cyclotron Centre , Calcutta, India. The powder of element was deposited on the aluminium backing. The samples were cut in to pieces of size 12mm x 12mm each and fixed with the help of zepon in acetone on aluminium holders having a circular

hole of diameter 8 mm in its centre. The zepon held the target foils to the target holder after the evaporation of acetone. The target foils with the holders were arranged in the form of a stack. In between the target foils, the aluminium foils of different thickness were also inserted to act as degrader.

Several irradiations were carried out using different stacks for different periods, depending upon the half lives of the residual nuclei of interest and as dictated by the convenience in following their activities over a period of time. Each of these foil stacks consisted self supporting metallic foils or deposited on Al backing by vacuum evaporation technique having purity greater than 99.99%, irradiated with 50 MeV alpha particles and in the case of gold another irradiation was carried out with 40 MeV alpha particles, using the Variable Energy Cyclotron, Calcutta (India). Several commercial grade aluminium foils of various thickness were used as energy degraders. The foil stack arrangements and the range - energy curves from which the mid-point beam energies are derived are shown in figures III.4 to III.7. The foil thickness in mg/cm^2 was determined in two ways, first by weighing an accurately measured area of the foil . The weight of the foil when divided by its area give the average thickness. This method is simple but due to non uniformities in the foil, it could lead to an under or over estimation of the thickness in the middle of the foil where the beam actually strikes. So in the second method, thickness directly measured using a micrometer, at different places and the average was taken. This average thickness in microns, multiplied by density gives the thickness of the foil in mg / cm^2 . The measured thickness by the two methods agreed fairly within the errors.

The incident α -particle flux can be determined in two ways, first by monitoring the α -particle beam with a Faraday Cup and calculating the total charge collected in it. In second indirect method, the flux measurement was made using

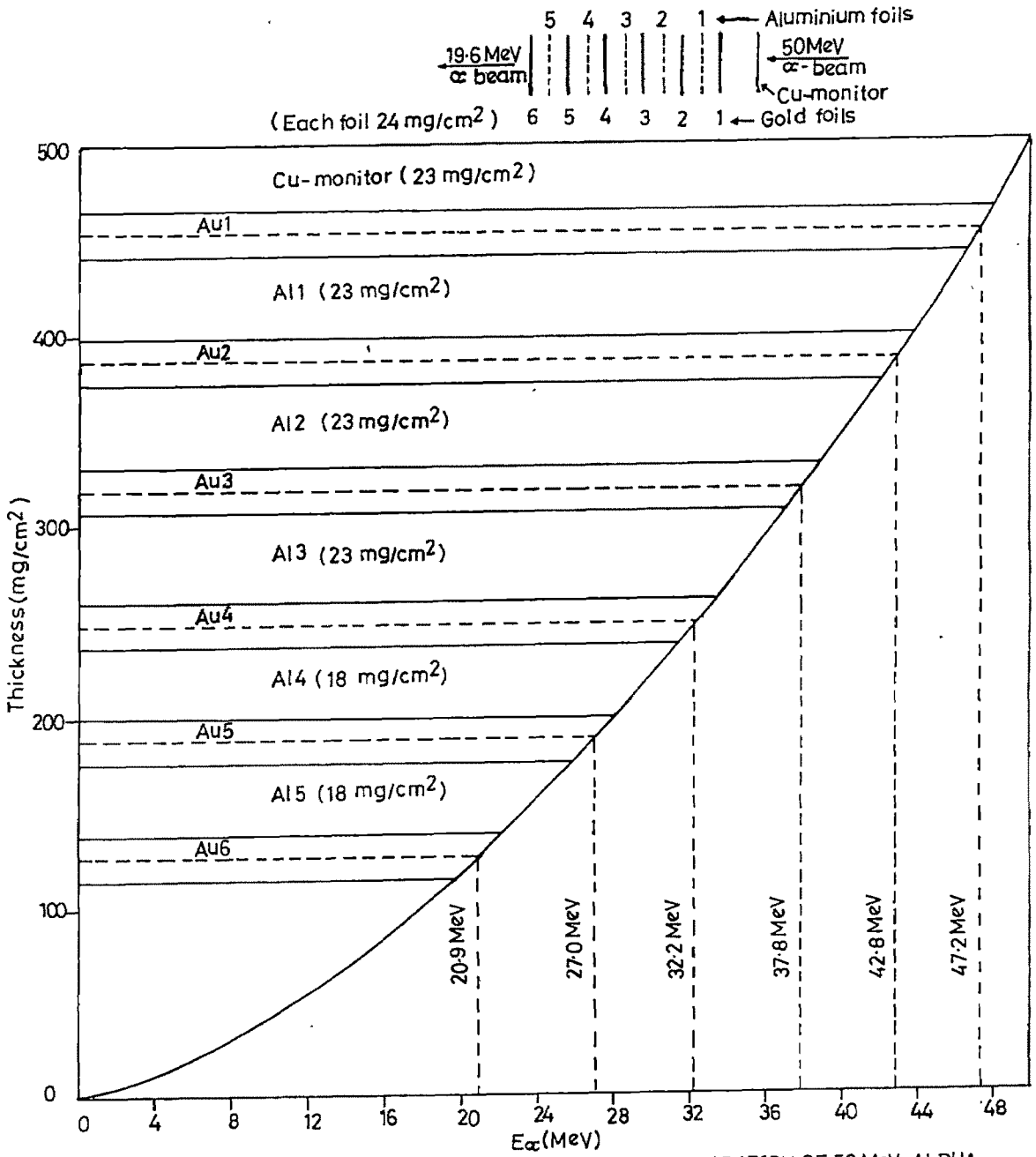


Fig.III.4a RANGE-ENERGY CURVE SHOWING THE ENERGY DEGRADATION OF 50 MeV ALPHA PARTICLES IN THE GOLD FOIL STACK.

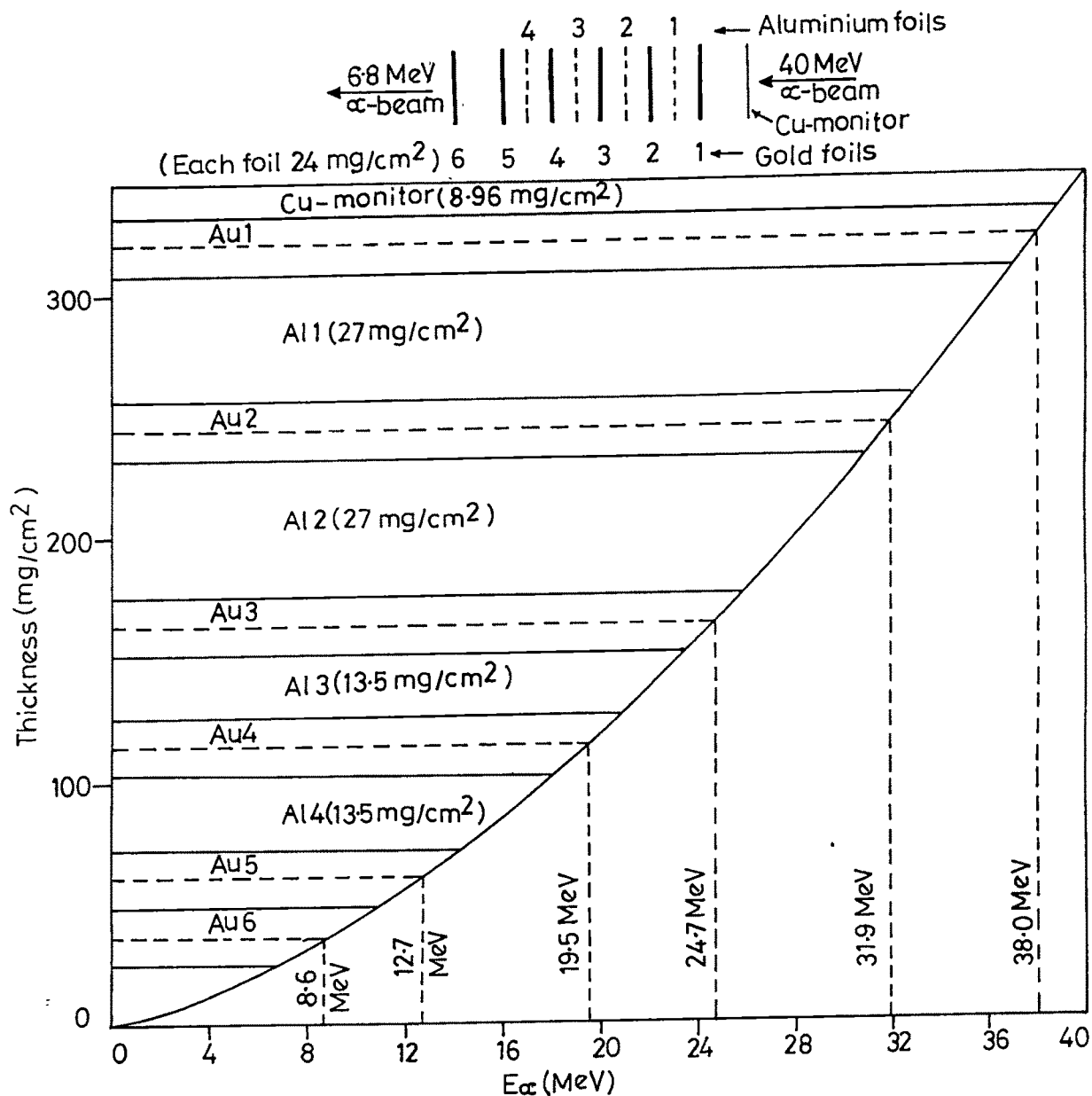


Fig.III.4b RANGE-ENERGY CURVE SHOWING THE ENERGY DEGRADATION OF 40 MeV ALPHA PARTICLES IN THE GOLD FOIL STACK.

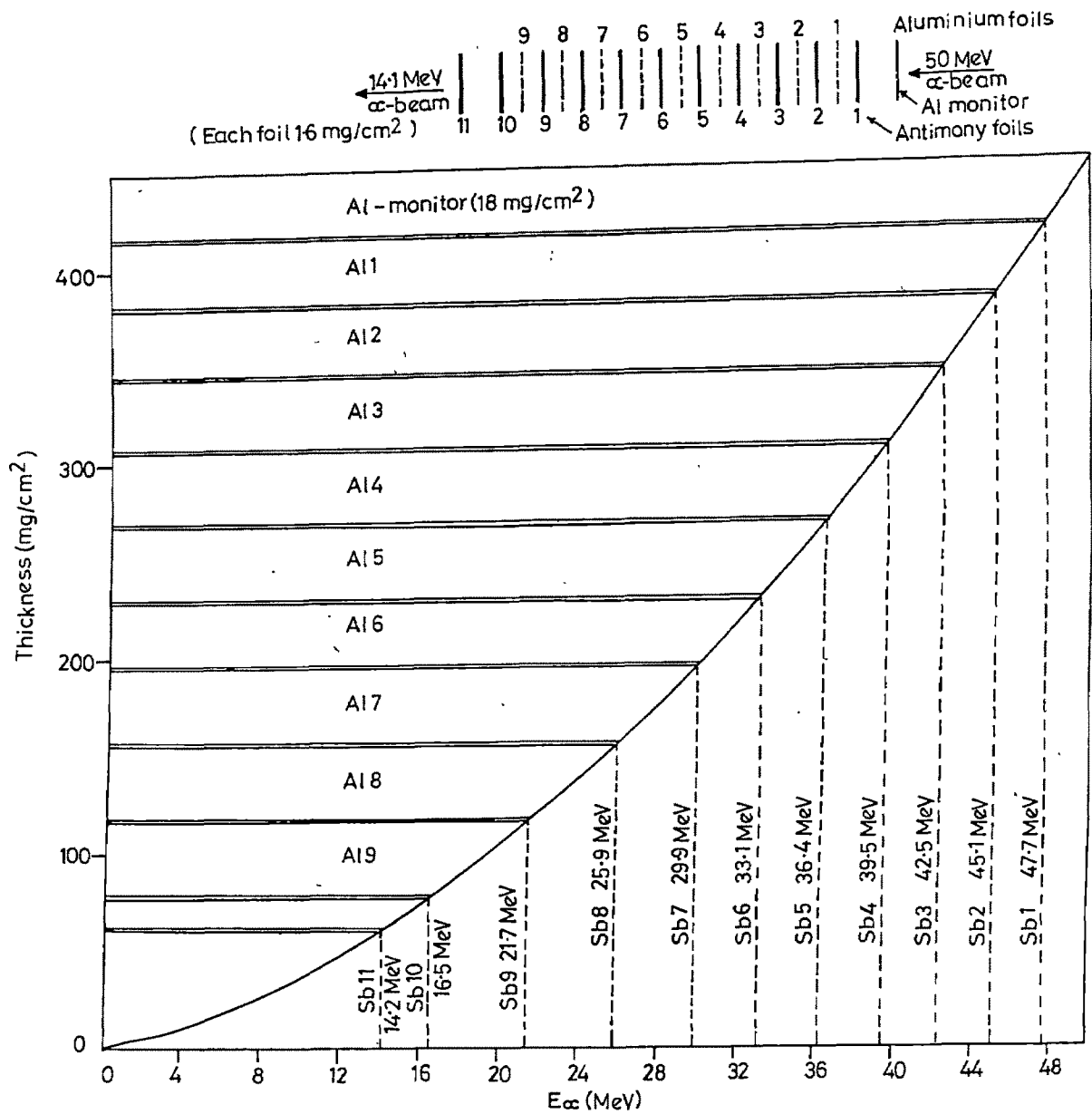


Fig III.5 RANGE-ENERGY CURVE SHOWING THE ENERGY DEGRADATION OF 50 MeV ALPHA PARTICLES IN THE ANTIMONY FOIL STACK

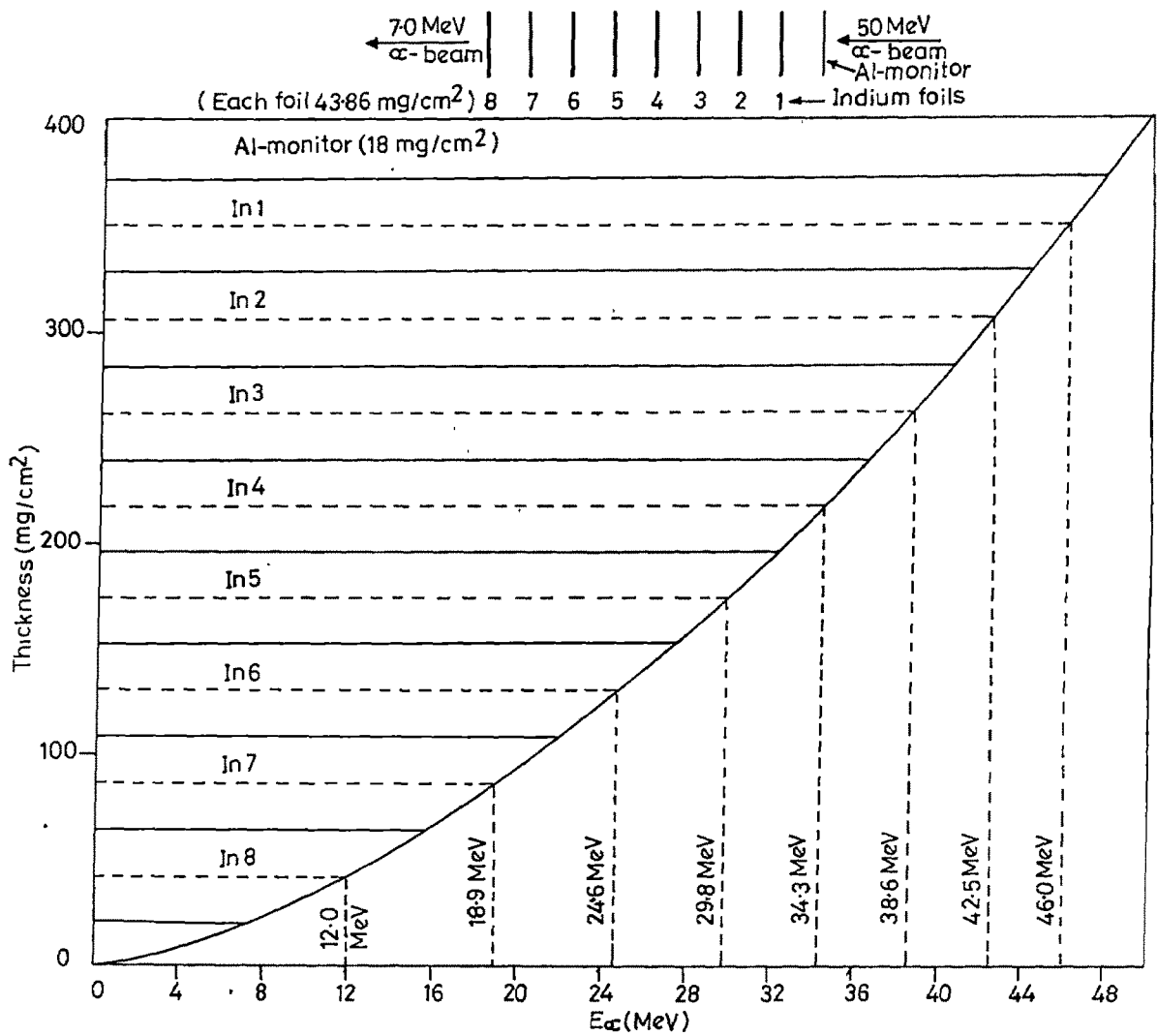


FIG.III.6 RANGE-ENERGY CURVE SHOWING THE ENERGY DEGRADATION OF 50 MeV ALPHA PARTICLES IN THE INDIUM FOIL STACK.

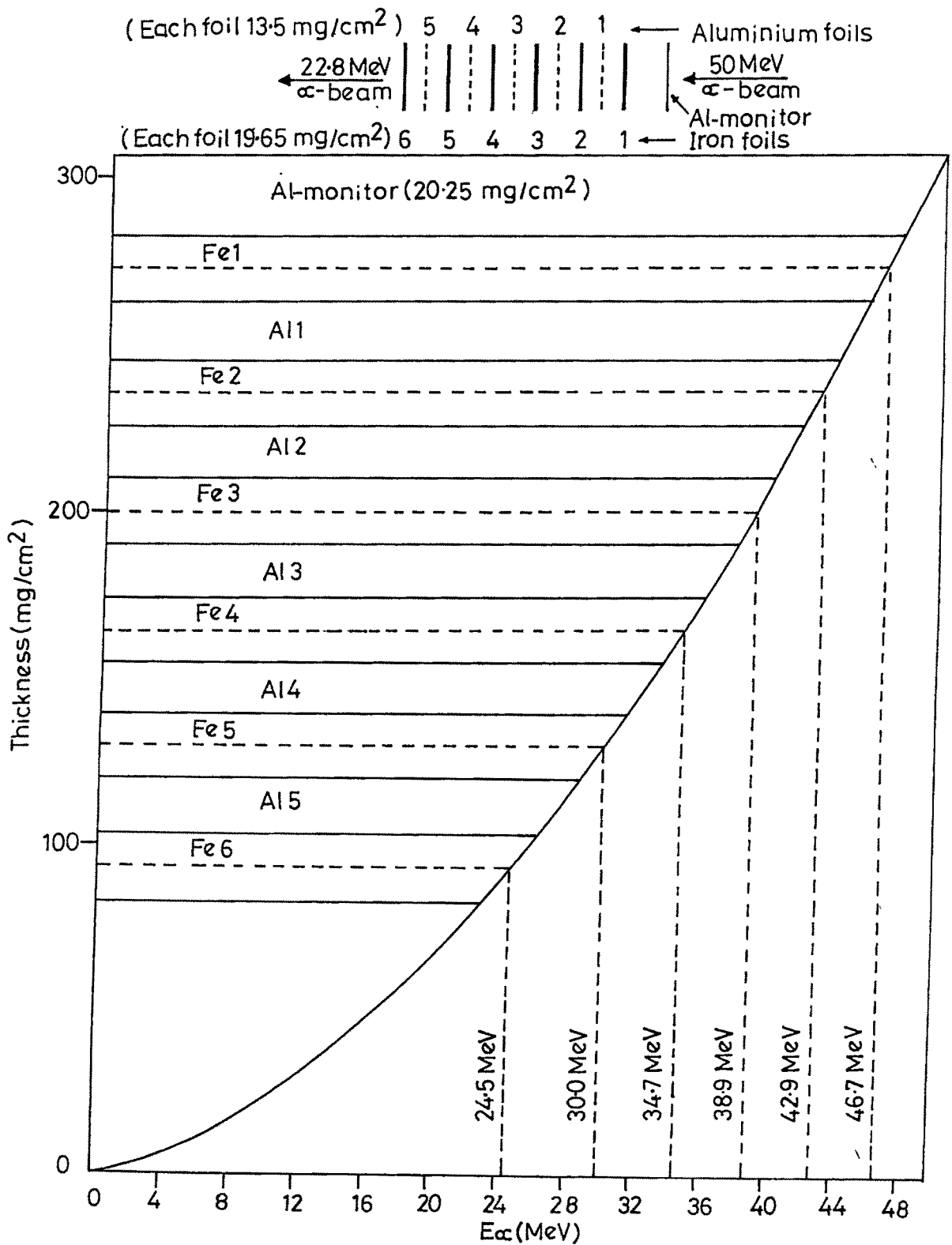


Fig.III.7 RANGE ENERGY CURVE SHOWING THE ENERGY DEGRADATION OF 50 MeV ALPHA PARTICLES IN THE IRON FOIL STACK

standard “monitor reactions”. At the front of each stack an aluminium or copper foil of suitable thickness was used as flux monitor. By measuring the activity of ^{24}Na which is produced in aluminium by the reaction $^{27}\text{Al}(\alpha, \alpha 2\text{pn})^{24}\text{Na}$ and assuming the well measured cross section /6/ for this reaction, the incident α -particle flux on each stack is deduced by back calculation. Since the beam current fluctuations during the irradiations were very small, the average incident flux in the present investigation was calculated by using the total charge collected in the Faraday Cup. In general, the two values agreed within 5%. Thus, with the knowledge of flux and detector efficiency, the absolute cross sections for the various reactions induced in the experimental targets, namely Au, Sb, In and Fe are determined in this work.

A few remarks are made below on the question of possible loss of beam intensity when it travels through material of the foil-stack. The beam intensity decreases as a function of the traversed foil thickness in a homogeneous stack according to the expression /7/ $\phi = \phi_0 \exp(-\sigma N_S)$; where ϕ_0 is the flux on the first foil, ϕ is the flux on the last foil, σ is the reaction cross section, N_S is the number of nuclei per unit area given by $\rho N_{av} / A$; where ρ is the density, N_{av} is the avogadro number and A is the atomic weight. For all experimental foil stacks, N_S is given by sum of the thickness of foils of the target element (T), aluminium degraders (Al) and monitor, i.e. $N_S = N_T + N_{Al}$. Assuming an upper limit for the total reaction cross section to be 2000 mb the maximum beam loss at the end of any of the experimental foil stack was to be less than 0.4 % and hence was neglected. The energy straggling at the end of the stack is always much smaller than the energy loss of the beam in the target foils. Hence the width of the folded energy distribution is not increased much. In reactions with the stack material the incoming beam will release a large amount of the low energy ($E \leq 10$ MeV) neutrons and protons, which can further react with the targets in the stack and disturb the yield mainly through

(n,p), (n, α), (p,n) and (p, α) reactions. However, the perturbation yield are mostly negligible.

The success of activation technique depends on the accuracy with which the induced β or γ activities can be measured in the activated foils, to identify the residual nuclei produced in different reactions. For reasons discussed in the previous section, the activity measurements have been carried out using HPGe detectors having resolution of 2 keV for 1332 keV photons. Photopeaks appear prominent and well separated in spectra taken with Germanium detectors because of high resolution and large peak-to-compton ratio. The γ -ray spectra of the standard ^{152}Eu source were taken in the same geometry for energy calibration and efficiency measurements. From the γ -ray spectra of irradiated foils, recorded on the multichannel analyser, a well resolved prominent photopeak characteristic of a product nucleus is usually selected, its total net area under the photopeak is measured to extract the cross section for the reaction in which the product nucleus is formed. Several γ -rays, apart from the prominent one, have also been used to identify the residual nucleus by studying the energies and relative intensities of these γ -rays and checking them with the literature /8/ values given for that residual nucleus.

III.3.1 Irradiation of Foil Stacks :

The stacks of each experimental foil was irradiated, using the Variable Energy Cyclotron at Calcutta (India). This is an indigenously built 224 cm AVF Cyclotron , used in the present experimental work. The maximum energy is given by $130 Q^2 / A$ where Q and A are the charge and mass of the ion. The energy of the particles from the machine can be varied by varying both the magnetic field and the radiofrequency electric field used for acceleration, hence the name 'Variable Energy

Cyclotron'. All the irradiations were performed in 0° port situated in cave I, as shown in the schematic diagram of the Variable Energy Cyclotron, figure III.8. A typical experimental setup for the stack irradiation is shown in the figure III.9. During the irradiation a low conductivity water (LCW) jet cooled both the flange as well as the stack. Beam diameter was limited to 5 mm by a central hole in a 6 mm thick tantalum sheet before the target chamber. The incident beam energy was determined from the operational parameters of the Cyclotron. Beam currents were of the order of 100-250 nA on the target stacks. The duration of irradiation and the beam current were selected according to the half lives of the residual nuclei of interest. The irradiation periods ranged from 0.5 hrs to 1.93 hrs given in table III.4. Although the half-lives of residual nuclei of interest range from 1.005 hrs to 271.6 days, the above periods of irradiation with the beam current mentioned (table III.4) were found to produce enough intense activities to give good statistics of counting.

III.3.2 Decay Characteristics :

The decay scheme data being used in the present analysis are summarised in tables III.5 to III.8 relevant to the target nuclei Au, Sb, In and Fe respectively. The tables indicate for each possible reaction, the Q- value , the residual nucleus formed, its half life, the energy and absolute abundance of the characteristic γ -ray transition , used in its identification and data analysis. The decay scheme data were taken from the "Table of Isotopes" compiled by Lederer and Shirley /8/. The Q-values are calculated using the values of mass excess given in the " Table of Isotopes".

III.3.3 Data Accumulation :

After the irradiation, the target foils were removed from the mount and kept in an isolated chamber , so as to avoid personnel exposure to the high dose of

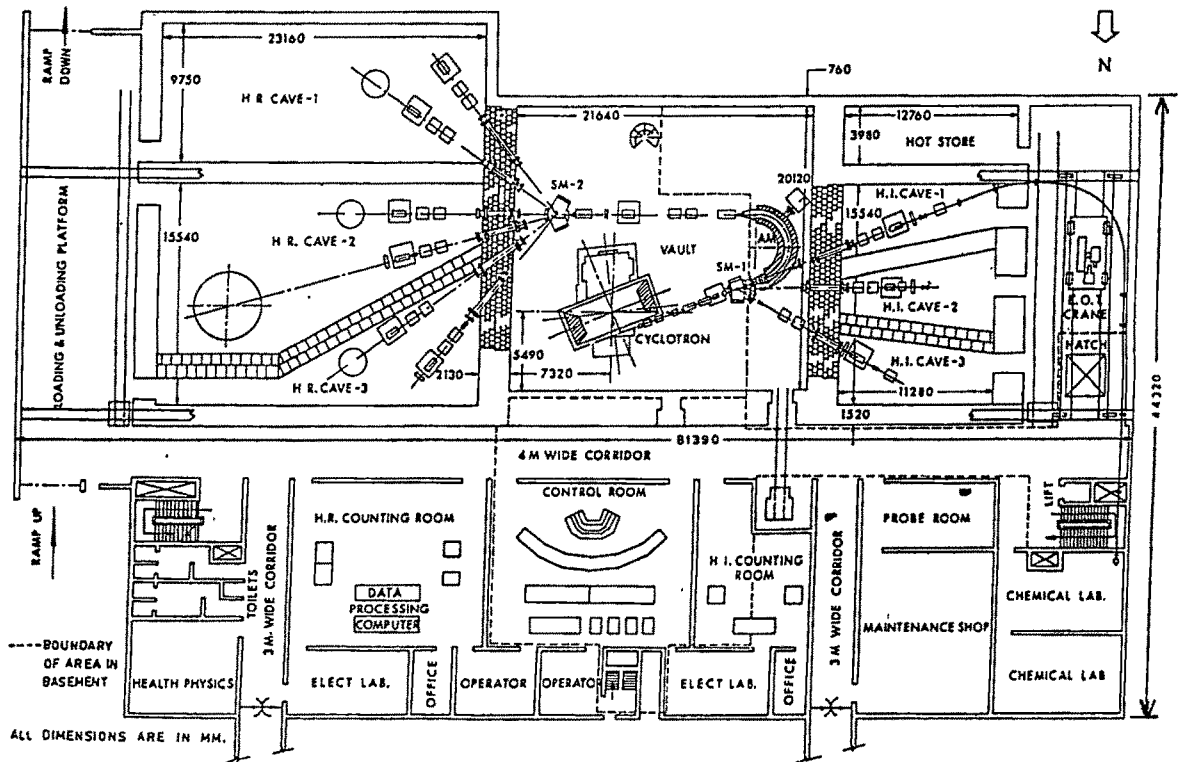


Fig. III. 8 Plan view of the Accelerator Bay in the VEC Building: The cyclotron is situated in 435 m² vault. The extracted beam enters through Switching Magnet 1 (SM-1) and Analysing Magnet (AM)—both unenergised—the 51 m² first High Intensity Cave (HI Cave-1), meant for production and radio-chemistry of isotopes. By energising SM-1, the beam enters either the 59 m² HI Cave 2 or 54 m² HI Cave 3 for radiation damage studies, neutron physics and low resolution nuclear physics and biological experiments. With AM energised, the extracted beam is analysed and by Switching Magnet-2 (SM-2), it enters any one of the six different channels located in three High Resolution

Caves. All nuclear physics and other high resolution experiments will be performed in either HR Cave-1 (226 m²) or HR Cave-2 (162 m²) or HR Cave-3 (155 m²).

The machine will be operated remotely from the Control Room (186 m²), while control of various experimental equipment and collection, monitoring and processing of experimental data generated in respective caves will be done in the corresponding High Intensity Counting Room (112 m²) and High Resolution Counting Room (186 m²). A versatile on-line computer will be located in HR Counting Room.

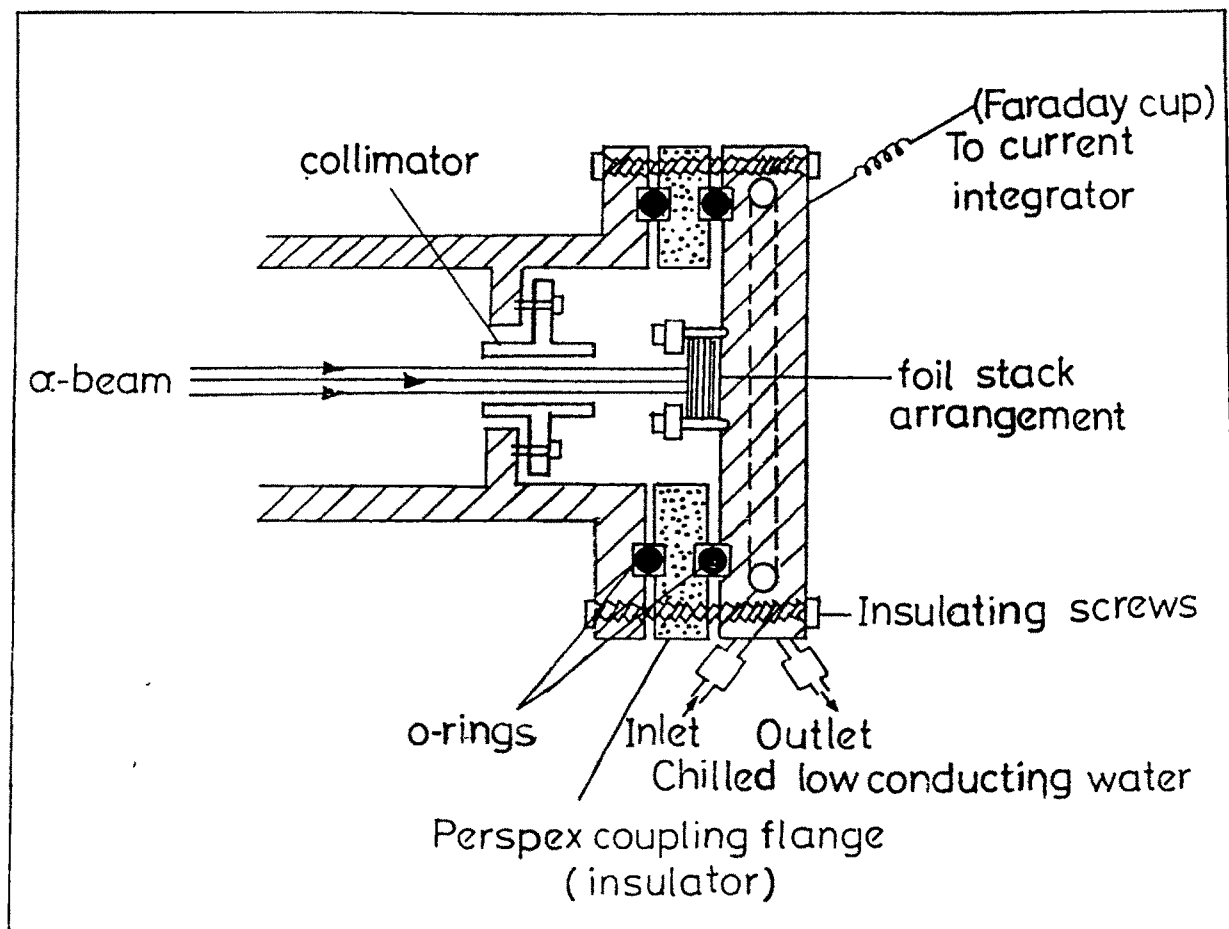


Fig.III.9 Experimental set up of stack foil activation technique

Table III.4 Details of the irradiations of the stacks :

Target element	Gold Au		Antimony Sb	Indium In	Iron Fe
Target foil thickness	24.0 mg/cm ²		1.6 mg/cm ²	43.86 mg/cm ²	19.65 mg/cm ²
Number of foils In the stack	6	6	11	8	6
Beam current	250 nA	250 nA	100 nA	100 nA	100 nA
Beam energy	50 MeV	40 MeV	50 MeV	50 MeV	50 MeV
Irradiation time	1.93 h	1.083h	0.5 h	1.416 h	1.45 h

Table III.5 Nuclear data used for the reaction in ^{197}Au /8/

Reaction	Product nucleus	Q-Value (MeV)	Half life $T_{1/2}$	Gamma Energy E_{γ}(keV)	Gamma intensity θ_{γ}(%)
$^{197}\text{Au} (\alpha,n)$	^{200}Tl	-09.73	26.10 h	0368	88.0
				0579	14.0
				1206	04.8
$^{197}\text{Au} (\alpha,2n)$	^{199}Tl	-17.80	07.42 h	0208	11.9
				0247	08.5
				0455	12.0
$^{197}\text{Au} (\alpha,3n)$	^{198}Tl	-25.87	05.30 h	0412	76.2
				0637	09.6
				0676	10.4
$^{197}\text{Au} (\alpha,2pn)$	^{198}Au	-23.78	02.69 d	0412	95.5
				1088	0.25
$^{197}\text{Au} (\alpha,\alpha n)$	^{196}Au	-08.00	06.15 d	0333	87.0
				0356	23.0

Table III.6 Nuclear data used for the reaction in $^{121,123}\text{Sb}$ /8/

Reaction	Product nucleus	Q-Value (MeV)	Half life $T_{1/2}$	Gamma Energy E_γ (keV)	Gamma intensity θ_γ(%)
$^{121}\text{Sb}(\alpha,n)$	^{124}I	-07.87	04.15 d	603	61.00
				723	10.66
$^{121}\text{Sb}(\alpha,2n)$	^{123}I	-15.33	13.02 h	159	82.90
				529	01.39
$^{121}\text{Sb}(\alpha,4n)$	^{121}I	-33.32	02.12 h	212	84.00
				319	01.04
				531	06.10
$^{121}\text{Sb}(\alpha,p3n)$	^{121}Te	-30.18	16.78 d	508	17.66
				573	80.30
$^{121}\text{Sb}(\alpha,\alpha n)$	^{120}Sb	-09.23	05.76 d	1023	99.10
				1172	100.0
$^{123}\text{Sb}(\alpha,3n)$	^{124}I	-23.64	04.15 d	603	61.00
				723	10.06
$^{123}\text{Sb}(\alpha,4n)$	^{123}I	-31.10	13.02 h	159	82.90
				529	01.39
$^{123}\text{Sb}(\alpha,\alpha 3n)$	^{120}Sb	-25.01	05.76 d	1023	99.10
				1172	100.0

Table III.7 Nuclear data used for the reaction in $^{113,115}\text{In}$ /8/

Reaction	Product nucleus	Q-Value (MeV)	Half life $T_{1/2}$	Gamma Energy E_γ (keV)	Gamma Intensity θ_γ (%)
$^{115}\text{In}(\alpha,n)$	^{118m}Sb	-07.44	5.000 h	0254	98.90
				1050	96.90
				1230	99.90
$^{115}\text{In}(\alpha,2n)$	^{117}Sb	-14.60	2.800 h	0159	86.10
				0861	00.28
				1020	00.09
$^{115}\text{In}(\alpha,3n)$	^{116m}Sb	-25.01	60.42 m	0543	52.10
				0973	72.30
				1294	100.0
$^{115}\text{In}(\alpha,2p)$	^{117m}In	-13.06	1.930 h	159	15.90
				315	16.90
$^{113}\text{In}(\alpha,n)$	^{116m}Sb	-08.69	1.005h	0543	52.10
				0973	72.30
				1294	100.0

Table III.8 Nuclear data used for the reaction in ^{56}Fe /8/

Reaction	Product nucleus	Q-Value (MeV)	Half life $T_{1/2}$	Gamma Energy E_γ (keV)	Gamma Intensity θ_γ(%)
$^{56}\text{Fe}(\alpha,3n)$	^{57}Ni	-26.32	036.00 h	0127 1378	12.90 77.60
$^{56}\text{Fe}(\alpha,4n)$	^{56}Ni	-36.56	006.10 d	0158 0480 0750	98.80 31.80 47.80
$^{56}\text{Fe}(\alpha,pn)$	^{58}Co	-13.70	070.78 d	0811	99.40
$^{56}\text{Fe}(\alpha,p2n)$	^{57}Co	-22.27	271.60 d	0122 0136	85.60 11.10
$^{56}\text{Fe}(\alpha,p3n)$	^{56}Co	-33.64	078.76 d	0847 1238	99.90 67.60

activity initially present in it. The time for which the irradiated foils were kept isolated is called cooling-off or waiting time. This is an important factor for the cross section calculation and hence should be measured carefully. Immediately after the cooling-off period, the gamma activities were measured one by one to an off-line counting system consisting of HPGe detector, multichannel analyser (MCA) along with the necessary electronics as shown in figure III.1.

The activity of residual nuclei were studied using 120 cm³ co-axial HPGe detector having resolution (2.0 keV FWHM for 1332 keV of ⁶⁰Co) in conjunction with 4096 channel multichannel analyser available at VECC, Calcutta (India) and IUC-DAEF Calcutta. Required bias voltage to the detectors were supplied from suitable power supplies. The output of the detector is d.c coupled to the pre-amplifier. The positive pulses from pre-amplifier were further amplified through a spectroscopy amplifier. These amplified pulses serve as input to the multichannel analyser. Data acquisition periods were varied from 200 sec to 4000 sec depending upon the intensity of activities. The residual nuclei with half-lives ranging from about 1.005 hr. to 271.6 days were observed by this technique. The energy calibration of spectrometer was made before and after the data acquisition using a standard multigamma source ¹⁵²Eu obtained from Radio Chemistry Division, VECC, Calcutta. The source-to-detector distance was selected such that the dead time of the detector was less than 5%. The details of parameters used in cross section calculations are given in the tables III.9 to III.27 for the prominent gamma ray of different reactions in each element.

III.3.4 Determination of Reaction Cross section :

From the gamma ray spectra recorded on the multichannel analyser, the area under the full energy peak of any characteristic gamma ray can be evaluated and

Table III.9 Experimental data for $^{197}\text{Au}(\alpha, n)^{200}\text{Tl}$ reaction :

$E_\alpha = 50 \text{ MeV}$

Incident Flux = 1.6047×10^{15} α -particles/cm² h

Time of Irradiation $t_i = 1.93 \text{ h}$

Gamma Energy $E_\gamma = 368 \text{ keV}$

Gamma Intensity $\theta_\gamma = 88.0 \%$

Half life = 26.1 h

Particle Energy E_α (MeV)	Waiting Time t_w (h)	Counting Time t_c (h)	Photo Peak Counts A_γ
20.90	86.78	1.11	175223
27.00	88.35	1.11	106191
32.20	89.65	1.11	50875
37.80	90.92	1.11	33865
42.80	92.28	1.11	25662
47.20	94.00	1.11	21543

$E_\alpha = 40 \text{ MeV}$

Incident Flux = 9.47×10^{15} α -particles/cm² h

Time of Irradiation $t_i = 1.083 \text{ h}$

Gamma Energy $E_\gamma = 368 \text{ keV}$

Gamma Intensity $\theta_\gamma = 88.0 \%$

Half life = 26.1 h

Particle Energy E_α (MeV)	Waiting Time t_w (h)	Counting Time t_c (h)	Photo Peak Counts A_γ
19.50	18.283	0.277	116975
24.70	17.783	0.277	141886
31.90	16.983	0.555	124753
38.00	16.150	0.555	82540

Table III.10 Experimental data for $^{197}\text{Au}(\alpha,2n)^{199}\text{Tl}$ reaction :

$E_\alpha = 50 \text{ MeV}$

Incident Flux = 1.6047×10^{15} α -particles/cm² h

Time of Irradiation $t_i = 1.93 \text{ h}$

Gamma Energy $E_\gamma = 455 \text{ keV}$

Gamma Intensity $\theta_\gamma = 12.0 \%$

Half life = 7.42 h

Particle Energy E_α (MeV)	Waiting Time t_w (h)	Counting Time t_c (h)	Photo Peak Counts A_γ
20.90	15.75	0.555	78302
27.00	15.08	0.555	439507
32.20	14.23	0.555	243649
37.80	13.50	0.555	96601
42.80	12.80	0.555	77263
47.20	12.15	0.555	53513

$E_\alpha = 40 \text{ MeV}$

Incident Flux = 9.47×10^{15} α -particles/cm² h

Time of Irradiation $t_i = 1.083 \text{ h}$

Gamma Energy $E_\gamma = 455 \text{ keV}$

Gamma Intensity $\theta_\gamma = 12.0 \%$

Half life = 7.42 h

Particle Energy E_α (MeV)	Waiting Time t_w (h)	Counting Time t_c (h)	Photo Peak Counts A_γ
19.50	18.283	0.277	43776
24.70	17.783	0.277	339917
31.90	16.983	0.555	677332
38.00	16.150	0.555	295215

Table III.11 Experimental data for $^{197}\text{Au}(\alpha,3n)^{198}\text{Tl}$ reaction :

$E_{\alpha} = 50 \text{ MeV}$

Incident Flux = $1.6047 \times 10^{15} \alpha\text{-particles/cm}^2 \text{ h}$

Time of Irradiation $t_i = 1.93 \text{ h}$

Gamma Energy $E_{\gamma} = 676 \text{ keV}$

Gamma Intensity $\theta_{\gamma} = 10.4 \%$

Half life = 5.3 h

Particle Energy E_{α} (MeV)	Waiting Time t_w (h)	Counting Time t_c (h)	Photo Peak Counts A_{γ}
32.20	14.23	0.555	188004
37.80	13.50	0.555	462122
42.80	12.80	0.555	366522
47.20	12.15	0.555	165344

$E_{\alpha} = 40 \text{ MeV}$

Incident Flux = $9.47 \times 10^{15} \alpha\text{-particles/cm}^2 \text{ h}$

Time of Irradiation $t_i = 1.083 \text{ h}$

Gamma Energy $E_{\gamma} = 676 \text{ keV}$

Gamma Intensity $\theta_{\gamma} = 10.4 \%$

Half life = 5.3 h

Particle Energy E_{α} (MeV)	Waiting Time t_w (h)	Counting Time t_c (h)	Photo Peak Counts A_{γ}
31.90	16.983	0.555	352711
38.00	16.150	0.555	1148795

Table III.12 Experimental data for $^{197}\text{Au}(\alpha,2\text{pn})^{198}\text{Au}$ reaction :

$E_{\alpha} = 50 \text{ MeV}$
 Incident Flux = $1.6047 \times 10^{15} \alpha\text{-particles/cm}^2\text{h}$
 Time of Irradiation $t_i = 1.93 \text{ h}$
 Gamma Energy $E_{\gamma} = 412 \text{ keV}$
 Gamma Intensity $\theta_{\gamma} = 95.5 \%$
 Half life = 2.69 d

Particle Energy E_{α} (MeV)	Waiting Time t_w (h)	Counting Time t_c (h)	Photo Peak Counts A_{γ}
37.80	90.92	1.11	17864
42.80	92.28	1.11	28437
47.20	94.00	1.11	45200

$E_{\alpha} = 40 \text{ MeV}$
 Incident Flux = $9.47 \times 10^{15} \alpha\text{-particles/cm}^2\text{h}$
 Time of Irradiation $t_i = 1.083 \text{ h}$
 Gamma Energy $E_{\gamma} = 412 \text{ keV}$
 Gamma Intensity $\theta_{\gamma} = 95.5 \%$
 Half life = 2.69 d

Particle Energy E_{α} (MeV)	Waiting Time t_w (h)	Counting Time t_c (h)	Photo Peak Counts A_{γ}
38.00	16.150	0.555	11987

Table III.13 Experimental data for $^{197}\text{Au}(\alpha,\alpha n)^{196}\text{Au}$ reaction :

$E_\alpha = 50 \text{ MeV}$

Incident Flux = 1.6047×10^{15} α -particles/cm² h

Time of Irradiation $t_i = 1.93 \text{ h}$

Gamma Energy $E_\gamma = 356 \text{ keV}$

Gamma Intensity $\theta_\gamma = 87.0 \%$

Half life = 6.15 d

Particle Energy E_α (MeV)	Waiting Time t_w (h)	Counting Time t_c (h)	Photo Peak Counts A_γ
32.20	89.65	1.11	58927
37.80	90.92	1.11	191232
42.80	92.28	1.11	373518
47.20	94.00	1.11	471256

$E_\alpha = 40 \text{ MeV}$

Incident Flux = 9.47×10^{15} α -particles/cm² h

Time of Irradiation $t_i = 1.083 \text{ h}$

Gamma Energy $E_\gamma = 356 \text{ keV}$

Gamma Intensity $\theta_\gamma = 87.0 \%$

Half life = 6.15 d

Particle Energy E_α (MeV)	Waiting Time t_w (h)	Counting Time t_c (h)	Photo Peak Counts A_γ
31.90	16.983	0.555	20550
38.00	16.150	0.555	79957

Table III.14 Experimental data for [$^{121}\text{Sb}(\alpha,n) + ^{123}\text{Sb}(\alpha,3n)] ^{124}\text{I}$ reactions:

$E_\alpha = 50 \text{ MeV}$

Incident Flux = $1.8454 \times 10^{15} \alpha\text{-particles/cm}^2 \text{ h}$

Time of Irradiation $t_i = 0.5 \text{ h}$

Gamma Energy $E_\gamma = 603 \text{ keV}$

Gamma Intensity $\theta_\gamma = 61.0 \%$

Half life = 4.15 d

Particle Energy E_α (MeV)	Waiting Time t_w (h)	Counting Time t_c (h)	Photo Peak Counts A_γ
14.20	36.00	0.555	1918
16.50	35.33	0.555	4439
21.70	34.68	0.555	1792
25.90	34.05	0.555	4434
29.90	33.40	0.555	18844
33.10	32.75	0.555	30965
36.40	32.08	0.555	36283
39.50	31.45	0.555	30289
42.50	30.80	0.555	22019
45.10	30.13	0.555	14768
47.70	29.43	0.555	8903

Table III.15 Experimental data for [$^{121}\text{Sb}(\alpha,2n) + ^{123}\text{Sb}(\alpha,4n)] ^{123}\text{I}$ reactions:

$E_\alpha = 50 \text{ MeV}$

Incident Flux = 1.8454×10^{15} α -particles/cm²h

Time of Irradiation $t_i = 0.5 \text{ h}$

Gamma Energy $E_\gamma = 159 \text{ keV}$

Gamma Intensity $\theta_\gamma = 82.90 \%$

Half life = 13.02 h

Particle Energy E_α (MeV)	Waiting Time t_w (h)	Counting Time t_c (h)	Photo Peak Counts A_γ
16.50	35.33	0.555	2576
21.70	34.68	0.555	92285
25.90	34.05	0.555	142273
29.90	33.40	0.555	130440
33.10	32.75	0.555	146376
36.40	32.08	0.555	87319
39.50	31.45	0.555	120471
42.50	30.80	0.555	213356
45.10	30.13	0.555	314617
47.70	29.43	0.555	367044

Table III.16 Experimental data for $^{121}\text{Sb}(\alpha,4n)^{121}\text{I}$ reaction :

$E_\alpha = 50 \text{ MeV}$

Incident Flux = 1.8454×10^{15} α -particles/cm²h

Time of Irradiation $t_i = 0.5 \text{ h}$

Gamma Energy $E_\gamma = 212 \text{ keV}$

Gamma Intensity $\theta_\gamma = 84.0 \%$

Half life = 2.12 h

Particle Energy E_α (MeV)	Waiting Time t_w (h)	Counting Time t_c (h)	Photo Peak Counts A_γ
36.40	2.50	0.139	1952
39.50	2.25	0.139	20134
42.50	2.06	0.139	83201
45.10	1.85	0.139	170638
47.70	1.58	0.139	228076

Table III.17 Experimental data for $^{121}\text{Sb}(\alpha,p3n)^{121}\text{Te}$ reaction :

$E_\alpha = 50 \text{ MeV}$

Incident Flux = 1.8454×10^{15} α -particles/cm²h

Time of Irradiation $t_i = 0.5 \text{ h}$

Gamma Energy $E_\gamma = 573 \text{ keV}$

Gamma Intensity $\theta_\gamma = 80.30 \%$

Half life = 16.78 d

Particle Energy E_α (MeV)	Waiting Time t_w (h)	Counting Time t_c (h)	Photo Peak Counts A_γ
39.50	31.45	0.555	484
42.50	30.80	0.555	1891
45.10	30.13	0.555	4321
47.70	29.43	0.555	6453

Table III.18 Experimental data for [$^{121}\text{Sb}(\alpha,\alpha n) + ^{123}\text{Sb}(\alpha,\alpha 3n)] ^{120}\text{Sb}$ reactions :

$E_\alpha = 50 \text{ MeV}$

Incident Flux = $1.8454 \times 10^{15} \alpha\text{-particles/cm}^2 \text{ h}$

Time of Irradiation $t_i = 0.5 \text{ h}$

Gamma Energy $E_\gamma = 1172 \text{ keV}$

Gamma Intensity $\theta_\gamma = 100.0 \%$

Half life = 5.76 d

Particle Energy E_α (MeV)	Waiting Time t_w (h)	Counting Time t_c (h)	Photo Peak Counts A_γ
25.90	34.05	0.555	57
29.90	33.40	0.555	412
33.10	32.75	0.555	730
36.40	32.08	0.555	776
39.50	31.45	0.555	805
42.50	30.80	0.555	936
45.10	30.13	0.555	1207
47.70	29.43	0.555	1575

Table III.19 Experimental data for $^{115}\text{In}(\alpha,n)^{118\text{m}}\text{Sb}$ reaction :

$E_\alpha = 50 \text{ MeV}$

Incident Flux = $0.9887 \times 10^{15} \alpha\text{-particles/cm}^2 \text{ h}$

Time of Irradiation $t_i = 1.416 \text{ h}$

Gamma Energy $E_\gamma = 1230 \text{ keV}$

Gamma Intensity $\theta_\gamma = 99.9 \%$

Half life = 5.0 h

Particle Energy E_α (MeV)	Waiting Time t_w (h)	Counting Time t_c (h)	Photo Peak Counts A_γ
18.90	6.333	0.139	22172
24.60	6.016	0.139	83732
29.80	5.800	0.086	22187
34.30	5.566	0.097	8740
38.60	5.333	0.083	4350
42.50	5.166	0.083	3082
46.00	4.916	0.139	3679

Table III.20 Experimental data for $^{115}\text{In}(\alpha,2n)^{1117}\text{Sb}$ reaction :

$E_\alpha = 50 \text{ MeV}$

Incident Flux = $0.9887 \times 10^{15} \alpha\text{-particles/cm}^2\text{h}$

Time of Irradiation $t_i = 1.416 \text{ h}$

Gamma Energy $E_\gamma = 159 \text{ keV}$

Gamma Intensity $\theta_\gamma = 86.1 \%$

Half life = 2.8 h

Particle Energy E_α (MeV)	Waiting Time t_w (h)	Counting Time t_c (h)	Photo Peak Counts A_γ
18.90	6.333	0.139	318892
24.60	6.016	0.139	4082330
29.80	5.800	0.086	1843492
34.30	5.566	0.097	966726
38.60	5.333	0.083	371271
42.50	5.166	0.083	239837
46.00	4.916	0.139	287858

Table III.21 Experimental data for [$^{113}\text{In}(\alpha,n) + ^{115}\text{In}(\alpha,3n)]^{116\text{m}}\text{Sb}$ reactions:

$E_\alpha = 50 \text{ MeV}$

Incident Flux = $0.9887 \times 10^{15} \alpha\text{-particles/cm}^2 \text{ h}$

Time of Irradiation $t_i = 1.416 \text{ h}$

Gamma Energy $E_\gamma = 973 \text{ keV}$

Gamma Intensity $\theta_\gamma = 72.3 \%$

Half life = 60.42 m

Particle Energy E_α (MeV)	Waiting Time t_w (h)	Counting Time t_c (h)	Photo Peak Counts A_γ
12.00	6.583	0.139	11
18.90	6.333	0.139	394
24.60	6.016	0.139	745
29.80	5.800	0.086	4384
34.30	5.566	0.097	43715
38.60	5.333	0.083	58238
42.50	5.166	0.083	50393
46.00	4.916	0.139	68727

Table III.22 Experimental data for $^{115}\text{In}(\alpha,2p)^{117\text{m}}\text{In}$ reaction :

$E_\alpha = 50 \text{ MeV}$

Incident Flux = $0.9887 \times 10^{15} \alpha\text{-particles/cm}^2\text{h}$

Time of Irradiation $t_i = 1.416 \text{ h}$

Gamma Energy $E_\gamma = 315 \text{ keV}$

Gamma Intensity $\theta_\gamma = 16.9 \%$

Half life = 1.93 h

Particle Energy E_α (MeV)	Waiting Time t_w (h)	Counting Time t_c (h)	Photo Peak Counts A_γ
24.60	6.016	0.139	76
29.80	5.800	0.086	171
34.30	5.566	0.097	503
38.60	5.333	0.083	823
42.50	5.166	0.083	1164
46.00	4.916	0.139	2327

Table III.23 Experimental data for $^{56}\text{Fe}(\alpha,3n)^{57}\text{Ni}$ reaction : $E_{\alpha} = 50 \text{ MeV}$ Incident Flux = 0.7071×10^{15} α -particles/cm²hTime of Irradiation $t_i = 1.45 \text{ h}$ Gamma Energy $E_{\gamma} = 1378 \text{ keV}$ Gamma Intensity $\theta_{\gamma} = 77.6 \%$

Half life = 36.0 h

Particle Energy E_{α} (MeV)	Waiting Time t_w (h)	Counting Time t_c (h)	Photo Peak Counts A_{γ}
30.00	34.97	0.555	405
34.70	33.70	0.555	1825
38.90	34.33	0.555	4056
42.90	32.46	0.555	6923
46.70	31.85	0.555	8124

Table III.24 Experimental data for $^{56}\text{Fe}(\alpha,4n)^{56}\text{Ni}$ reaction : $E_{\alpha} = 50 \text{ MeV}$ Incident Flux = 0.7071×10^{15} α -particles/cm²hTime of Irradiation $t_i = 1.45 \text{ h}$ Gamma Energy $E_{\gamma} = 750 \text{ keV}$ Gamma Intensity $\theta_{\gamma} = 47.8 \%$

Half life = 6.10 d

Particle Energy E_{α} (MeV)	Waiting Time t_w (h)	Counting Time t_c (h)	Photo Peak Counts A_{γ}
42.90	32.46	0.555	563
46.70	31.85	0.555	1864

Table III.25 Experimental data for $^{56}\text{Fe}(\alpha, \text{pn})^{58}\text{Co}$ reaction :

$E_\alpha = 50 \text{ MeV}$

Incident Flux = 0.7071×10^{15} α -particles/cm² h

Time of Irradiation $t_i = 1.45 \text{ h}$

Gamma Energy $E_\gamma = 811 \text{ keV}$

Gamma Intensity $\theta_\gamma = 99.4 \%$

Half life = 70.78 d

Particle Energy E_α (MeV)	Waiting Time t_w (h)	Counting Time t_c (h)	Photo Peak Counts A_γ
24.50	35.58	0.555	25453
30.00	34.97	0.555	26732
34.70	33.70	0.555	14785
38.90	34.33	0.555	9428
42.90	32.46	0.555	5853
46.70	31.85	0.555	3785

Table III.26 Experimental data for $^{56}\text{Fe}(\alpha, p2n)^{57}\text{Co}$ reaction :

$E_{\alpha} = 50 \text{ MeV}$
 Incident Flux = $0.7071 \times 10^{15} \alpha\text{-particles/cm}^2 \text{ h}$
 Time of Irradiation $t_i = 1.45 \text{ h}$
 Gamma Energy $E_{\gamma} = 122 \text{ keV}$
 Gamma Intensity $\theta_{\gamma} = 85.6 \%$
 Half life = 271.6 d

Particle Energy E_{α} (MeV)	Waiting Time t_w (h)	Counting Time t_c (h)	Photo Peak Counts A_{γ}
30.00	1751.92	0.555	2240
34.70	1751.32	0.555	17960
38.90	1750.42	1.111	62900
42.90	1748.98	1.111	74698
46.70	1747.82	1.111	55290

Table III.27 Experimental data for $^{56}\text{Fe}(\alpha, p3n)^{56}\text{Co}$ reaction :

$E_{\alpha} = 50 \text{ MeV}$
 Incident Flux = $0.7071 \times 10^{15} \alpha\text{-particles/cm}^2 \text{ h}$
 Time of Irradiation $t_i = 1.45 \text{ h}$
 Gamma Energy $E_{\gamma} = 847 \text{ keV}$
 Gamma Intensity $\theta_{\gamma} = 99.9 \%$
 Half life = 78.76 d

Particle Energy E_{α} (MeV)	Waiting Time t_w (h)	Counting Time t_c (h)	Photo Peak Counts A_{γ}
38.90	1750.42	1.111	118
42.90	1748.98	1.111	977
46.70	1747.82	1.111	2943

related to the actual number of residual nuclei formed in the reaction and hence to the nuclear reaction cross section.

Let a beam of α -particles be incident on a thin foil of target material of thickness x and density ρ . Let the incident flux be ϕ particles per unit area in unit time. Let the number of target nuclei per unit area be N_T . Then with each target nucleus we can associate an effective area ' σ ', the cross section, such that if the incident particle passes through this area ' σ ' around a particular target nucleus, nuclear reaction is said to occur.

When a target nuclide, under irradiation in a constant α -particle flux, produces a radionuclide with a disintegration constant λ , the rate of production of radioactive atoms is the steady rate, $\sigma N_T \phi$ from α -particle bombardment minus the rate of radioactive decay, $\lambda N(t)$ i.e.

$$\frac{dN(t)}{dt} = \sigma N_T \phi - \lambda N(t); \quad (1)$$

where ϕ is the flux, λ is the disintegration constant, σ is the cross section for the reaction in which the radioactive residual nucleus is formed and N_T is the number of target nuclei per unit area exposed to the beam. $N(t)$ is the number of radioactive atoms present at any time t .

Eqn. (1) may be written as

$$\frac{dN(t)}{dt} + \lambda N(t) = \sigma N_T \phi \quad (2)$$

Eqn. (2) is the first order differential equation of the form

$$\frac{dy}{dx} + Py = Q \quad (\text{i.e. Leibnitz equation}).$$

The solution of this equation is given by

$$y = \exp\left(-\int P dx\right) \int Q \exp\left(\int P dx\right) dx + C' \exp\left(-\int P dx\right)$$

where C' is the constant of integration.

Similarly solution of eqn. (2) is given by

$$\begin{aligned} N(t) &= \exp\left(-\int \lambda dt\right) \int \sigma N_T \phi \exp\left(\int \lambda dt\right) dt + C' \exp\left(-\int \lambda dt\right) \\ &= \exp(-\lambda t) \int \sigma N_T \phi \exp(\lambda t) dt + C' \exp(-\lambda t) \\ &= \exp(-\lambda t) \sigma N_T \phi \frac{\exp \lambda t}{\lambda} + C' \exp(-\lambda t) \\ &= \frac{\sigma N_T \phi}{\lambda} + C' \exp(-\lambda t) \end{aligned} \quad (3)$$

Let us define the boundary condition, that when $t=0$, $N(t)=0$ then

$$C' = \frac{-\sigma N_T \phi}{\lambda}$$

substituting the value of C' in eqn.(3)

$$N(t) = \frac{\sigma N_T \phi}{\lambda} - \frac{\sigma N_T \phi}{\lambda} (e^{-\lambda t}) = \frac{\sigma N_T \phi}{\lambda} (1 - e^{-\lambda t})$$

This is the growth equation for the radioactive residual nuclei formed in the reaction, during the period of irradiation.

If t_i is the time of irradiation then the number of residual nuclei present, $N(t_i)$ at the end of the irradiation (t_i) is given by

$$N(t_i) = \frac{\sigma N_T \phi}{\lambda} (1 - e^{-\lambda t_i}) \quad (4)$$

Since the gamma counting is performed after time t' , during this time activity is given by

$$\frac{dN(t')}{dt'} = \lambda N(t') \quad (5)$$

where $N(t') = N(t_i)e^{-\lambda t'}$; then eqn. (5) can be written as

$$dN(t') = \lambda N(t_i)e^{-\lambda t'} dt' \quad (6)$$

If t_w is the cooling - off time or the time elapsed after the end of irradiation and start of counting and t_c is the data accumulation time then the number of radioactive nuclei that have decayed during the period t_w and $t_w + t_c$ is

$$\int_{t_w}^{t_w + t_c} dN(t') = \lambda \int_{t_w}^{t_w + t_c} N(t_i)e^{-\lambda t'} dt' \quad (7)$$

Using eqn.(4) the above eqn. (7) gives

$$\int_{t_w}^{t_w + t_c} dN(t') = \frac{\lambda \sigma N_T \phi}{\lambda} (1 - e^{-\lambda t_i}) \int_{t_w}^{t_w + t_c} e^{-\lambda t'} dt'$$

$$[N(t')]_{t_w}^{t_w + t_c} = \sigma N_T \phi \frac{(1 - e^{-\lambda t_i})}{(-\lambda)} [e^{-\lambda t'}]_{t_w}^{t_w + t_c}$$

The L.H.S of above eqn. actually gives the number of radioactive nuclei that have decayed during the collection time t_c and observed through their characteristic gamma rays as the area under photo-peak A_γ , with appropriate efficiency.

$$\frac{A_\gamma}{\mathcal{G}_\gamma P_\gamma} = \frac{\sigma N_T \phi (1 - e^{-\lambda t_i})}{\lambda} [e^{-\lambda t_w} - e^{-\lambda(t_w + t_c)}]$$

where θ_γ is the absolute abundance of gamma ray and P_γ is the photo-peak efficiency of the detector for that gamma ray.

$$\frac{A_\gamma}{\mathcal{G}_\gamma P_\gamma} = \frac{\sigma N_T \phi (1 - e^{-\lambda t_i})}{\lambda} e^{-\lambda t_w} (1 - e^{-\lambda t_c})$$

Therefore

$$\sigma = \frac{A_\gamma \lambda}{\theta_\gamma P_\gamma N_T \phi (1 - e^{-\lambda t_i}) (e^{-\lambda t_w}) (1 - e^{-\lambda t_c})} \quad (8)$$

where N_T is the number of nuclei in the target given by

$$N_T = \frac{W_i P_i N_{av}}{A_i}$$

where W_i is the weight of the foil per unit area, P_i is the isotopic abundance of the target nuclei, A_i is the mass number of the target nucleus and N_{av} is the Avagadro number ($= 6.023 \times 10^{23}$ atoms/mole).

$$\therefore \sigma = \frac{A_i A_\gamma \lambda}{\phi \theta_\gamma P_\gamma W_i P_i N_{av} \phi (1 - e^{-\lambda t_i}) (e^{-\lambda t_w}) (1 - e^{-\lambda t_c})} \quad (9)$$

The factor $(A_\gamma \lambda e^{\lambda t_w}) / (1 - e^{-\lambda t_c})$ is the count rate of the induced activity just at the stop of irradiation. The factor, $(1 - e^{-\lambda t_i})$ is called saturation correction, accounts for the decay of the activity during the irradiation.

In this equation quantities like θ_γ , P_i and λ are taken from the "Table of Isotopes" /8/. The photo-peak efficiency P_γ of the characteristic gamma ray was taken from the detector efficiency curve as already discussed earlier. Photo-peak area for a particular gamma ray is given by the sum $A_\gamma = \sum (N_i - B_i)$; where N_i is the observed counts in a channel i in the peak and B_i is the background counts in the

same channel, the summation being carried out from the low energy end to the high energy end of the photopeak. Usually the background B, is obtained by smoothly joining the two ends of the peak and interpolating in between. The above method of cross section evaluation is valid in straight forward cases, i.e. when the activity of a particular radioactive isotope can be studied in isolation without any interference of disturbing γ -rays or contribution from other product nuclei.

III.3.5 Isotopic Reaction Contribution :

Consequent on the use of natural target, which has two isotopes, the isotopic contributions arise in the production of a given final nucleus through different reaction channels, for example antimony having two isotopes with mass number ^{121}Sb and ^{123}Sb leading to isotopic contributions, i.e. ^{124}I is formed in $^{121}\text{Sb}(\alpha, n)$ and $^{123}\text{Sb}(\alpha, 3n)$ reactions.

However, more often than not, it turns out that at a given energy only one of the two reaction channels is predominant and other is a small contribution. One of the two vanishes, if the energy happens to be less than the threshold energy for that reaction. On this basis the experimentally measured weighted average cross sections can be easily interpreted using the formula,

$$\langle \sigma \rangle = \bar{A}_i \left[\frac{P_1 \sigma_1}{A_1} + \frac{P_2 \sigma_2}{A_2} \right] \quad (10)$$

where \bar{A}_i is the average atomic weight of antimony. $P_1 A_1$ and $P_2 A_2$ are the percentage abundance and mass number of two isotopes of the natural target in respective order ; and σ_1 and σ_2 are the individual cross sections of the reactions from two isotopes respectively. The two contribution can be separated quite accurately using either the known theoretical ratio of cross section /9/ or by

subtracting the contribution of one of the reactions measured with an enriched isotope/10/.

Efforts were made to separate the individual contributions of the reactions using the theoretical excitation function in the equations.

$$\sigma_{(\alpha,n)}^{121} = \frac{A\gamma\lambda}{\left[\frac{P_i^{121}}{A_i^{121}} + \frac{P_i^{123} (\sigma_{(\alpha,3n)}^{123} / \sigma_{(\alpha,n)}^{121})_{theo.}}{A_i^{123}} \right] \phi\theta\gamma P\gamma W i N a v (1 - e^{-\lambda t i})(e^{-\lambda t w})(1 - e^{-\lambda t c})}$$

(11)

$$\sigma_{(\alpha,3n)}^{123} = \frac{A\gamma\lambda}{\left[\frac{P_i^{123}}{A_i^{123}} + \frac{P_i^{121} (\sigma_{(\alpha,n)}^{121} / \sigma_{(\alpha,3n)}^{123})_{theo.}}{A_i^{121}} \right] \phi\theta\gamma P\gamma W i N a v (1 - e^{-\lambda t i})(e^{-\lambda t w})(1 - e^{-\lambda t c})}$$

(12)

where the cross section ratio $[\sigma_{(\alpha,3n)}^{123} / \sigma_{(\alpha,n)}^{121}]_{theo.}$ and its inverse are taken from the theoretical calculations based on hybrid model which predicts the shape and absolute value of the experimentally measured excitation function. Below the threshold energy of $^{123}\text{Sb}(\alpha,3n)$ reaction, the value of $^{123}\text{Sb}(\alpha,3n)$ will be zero and hence the second factor in the square bracket will be zero and therefore eqn. (11) reduces to eqn. (9). Similar analysis is carried out for other reaction. The method of evaluation of reaction cross section using eqn.(9) is applicable in straight forward cases where the activity of the residual nucleus alone is measured.

III.3.6 Isobaric Precursor Contribution :

More often than not, nuclear reactions occur in which two genetically related product nuclei (e.g. isobars or isomers) are formed with measurable half lives and

one of them the residual nucleus (daughter) is continuously fed by the other, the parent nucleus by radioactive decay . In such cases, the simple expression eqn. (9) given above can not be employed to determine the cross section of the daughter nucleus , since it does not take into account the contribution from the feeding precursor nucleus (parent nucleus). Therefore the cross section σ_p for the production of parent nucleus is first determined using eqn.(9) . Then the following new expression /11/ which accounts for the contribution from the parent activity to the daughter activity, is employed to determine the cross section σ_d for the formation of the daughter nucleus.

$$\begin{aligned} \frac{A_i A_\gamma}{\phi \theta \gamma P \gamma W_i P_i N_{av}} &= \sigma_p (1 - e^{-\lambda_p t_i}) \frac{\lambda_d}{\lambda_d - \lambda_p} \left\{ \frac{e^{-\lambda_p t_w} - e^{-\lambda_p (t_w + t_c)}}{\lambda_p} - \frac{e^{-\lambda_d t_w} - e^{-\lambda_d (t_w + t_c)}}{\lambda_d} \right\} + \\ \sigma_p &\left\{ 1 - \frac{\lambda_d}{\lambda_d - \lambda_p} e^{-\lambda_p t_i} - \frac{\lambda_p}{\lambda_p - \lambda_d} e^{-\lambda_d t_i} \right\} \left\{ \frac{e^{-\lambda_d t_w} - e^{-\lambda_d (t_w + t_c)}}{\lambda_d} \right\} + \\ \sigma_d (1 - e^{-\lambda_p t_i}) &\left\{ \frac{e^{-\lambda_d t_w} - e^{-\lambda_d (t_w + t_c)}}{\lambda_d} \right\} \end{aligned} \quad (13)$$

(See Appendix for derivation)

III.3.7 Determination of Alpha Particle Flux :

In evaluating the cross section of a particular nuclear reaction, flux of the incident alpha particles is an important quantity which has to be determined with reasonable accuracy . There are two ways in which alpha particle flux can be determined.

(I) It can be directly determined by measuring the total charge of the incident α - particles using Faraday Cup and current integrator. If the total charge collected is Q and t_i is the irradiation time, then $\phi = Q / 2 e t_i$ gives the number of α -particles falling on the target per unit time. The charge state of alpha particle is 2 and e is the electronic charge.

Although in principle the Faraday Cup is a simple device, several sources of error may be present. For example, the region of the Cup in which the beam stops will be a source of secondary electrons which, if they escape, will make the beam intensity overestimated. Therefore, the length of the Cup should be large compared to the diameter of the entrance aperture to ensure a negligible solid angle for the escape of secondary electrons. It may be noted that the places where ever the α - beam strikes (like collimators etc.) are all sources of secondary electrons. The latter has to be prevented from entering the Faraday Cup by proper design. Also, the current collected by the Cup should be measured by a current integrator with a feedback to hold the Cup potential near ground at all times.

(II) In the second method, the incident flux is determined indirectly by using a standard monitor reaction, whose cross section is accurately measured and is available in literature /6/. An aluminium foil of suitable thickness was placed in front of each stack and irradiated together with the experimental foils. The gamma rays activity of the aluminium foil was measured in the usual way. The reaction $^{27}\text{Al} (\alpha, \alpha 2\text{pn}) ^{24}\text{Na}$ ($t_{1/2} = 15.05$ hours) was used as monitor reaction for flux calculation.

Using the characteristic photopeak of 1369 keV of ^{24}Na and standard monitor cross section σ' for the reaction $^{27}\text{Al} (\alpha, \alpha 2\text{pn})$, the flux ϕ of the primary α - particle beam is calculated with the help of equation

$$\phi = \frac{A_i' A_{\gamma}' \lambda'}{\sigma' \theta_{\gamma}' P_{\gamma}' W_i' P_i N_{av} (1 - e^{-\lambda' t_i'}) (e^{-\lambda' t_w'}) (1 - e^{-\lambda' t_c'})} \quad (14)$$

where all the primed symbols have their usual meaning now with reference to the monitor aluminium foil, the value of monitor cross section σ' corresponding to the energy of incident alpha particle beam is taken from literature /6/ and used in the above equation.

III.3.8 Error Analysis :

The overall error in the present measurement of cross section may be divided into the following categories.

(1) In order to estimate the number of nuclei in the sample and to check the thickness and uniformity of the sample, pieces of sample foils of dimension 12 mm × 12 mm were weighted on an electronic microbalance and the thickness of each foil were calculated. This non uniformity in the foil thickness may introduce a 1-2 % error(δ_1).

(2) Variation in the incident α -particle flux may introduce some uncertainty in the final calculation of the cross section. The error(δ_2) in the measurement of the total charge collected in the Faraday Cup due to beam current fluctuation and others to be estimated 4-5%.

(3) The calculated detection efficiency may be inaccurate due to the uncertainty in the spectroscopic data of the standard source and the statistical errors in the counts and also due to geometrical arrangement. No corrections were applied

for the uncertainty in the spectroscopic data. However, the statistical error (δ_3) in counting the characteristic gamma rays of the standard ^{152}Eu source and the geometrical arrangement used for the efficiency calculations was estimated to be 3-4%.

(4) The dead time in the pulse processing electronics may lead to a loss of counts, the sample-detector distance was suitably adjusted to keep the dead time low ($< 5\%$) and corrections for it were applied accordingly in the counting rates. However the error (δ_4) introduced in the determination of photo peak area of the characteristic gamma rays were within the limits of 1-4% in the best and worst cases. Therefore, the total error in the measured cross section is $\sqrt{\sum \delta_i^2}$ and found to be less than 8%.

However, the above mentioned errors do not include uncertainties of the nuclear data (e.g. half lives of residual nuclei, branching ratio etc.) used in the analysis and summarised in table III.28.

Other factors which may influence the cross section measurements are the following.

(I) In the irradiation experiment the initial energy was degraded down to around one-third of its original value. As the α - beam traverses the stack material, the initial beam intensity may become disturbed. This decrease in beam intensity may introduce certain errors. The maximum beam loss at the end of a high z-stack is calculated to be less than 0.4 % and hence can be neglected.

Table III.28 Uncertainties in the measured cross sections :

Quantity measured or taken from literature.	Percentage error in the quantity.
Photo peak area of the characteristic γ -rays	1-4%
Relative error in photo peak efficiency	3-4%
Thickness of foils	1-2%
Beam current	4-5%
Irradiation time, waiting time ,counting time	negligible
Isotopic weight and abundance	negligible
Overall error in the measurement	less than 8%

(II) Straggling effects may introduce some errors but are neglected because for alpha particles the energy straggling at the end of the stack is always much smaller than the energy of the beam in the target foil itself. It was pointed out by Ernst et al /7/ that a large number of low energy neutrons may be released as the beam traverses through the stack of the foils and this in turn may disturb the yield. However, this distributing yield is also negligible.

References :

- /1/ A.J. Tavendale and G.T Ewan, Nucl.Inst. & Meth. **25**, 185 (1963).
- /2/ K. Debertin, Nucl.Inst. & Meth. **158**, 479 (1979).
- /3/ K.Debertin and Ulrich Schotzig, Nucl.Inst. & Meth. **158**, 471 (1979).
- /4/ Orear. Jay, Report CLNS 82/511 July 28 (1982).
- /5/ C.F.Williamson, J.P.Boujot and J. Picard, Centre d'Etudes, Nucleaire d Sacy Report CEA-R 3042 (1966).
- /6/ H.J. Probst, S.M.Qaim and R.Weinreich, Int.J. Applied Radiation & Isotopes **27**, 431(1976).
- /7/ J.Ernst, R.Ibowski, H.Klampil, H.Machner, T.Mayer .Kuckuk and R.Shanz , Z.Phys. **A308**, 301(1982).
- /8/ C.M. Lederer and V.S. Shirley, Table of Isotopes, John Wiley and Sons., New York (1978).
- /9/ N.L.Singh , S.Agarwal , L.Chaturvedi and J.Rama Rao, Nucl.Inst & Meth. **B24/25**, 480 (1987).
- /10/ P.Misaelides and H.Muenzel, J.Inorg. Nucl. Chem. **42**, 937 (1980).
- /11/ S. Mukherjee, N.L. Singh and J. Rama Rao, Pramana J. Phys. **41**, 311 (1993).